**CENTRO DE INVESTIGACIONES
EN OPTICA, A.C.**

"GENERACIÓN DE HACES ESTRUCTURADOS PARCIALMENTE COHERENTES"

Versión definitiva. Incluye cambios sugeridos por revisores.

Tesis que para obtener el grado de Maestra en Ciencias (Óptica)

Presenta: *Maria Fernanda Arvizu Soto*

Director de Tesis: *Dr. Carmelo Rosales-Guzmán*

Vo. Bo.

León · Guanajuato · México
16 de enero de 2024

Abstract

Through the manipulation of the intensity, polarization and phase on a light field is how we can obtain structured light. There are several techniques for structuring light in the high spatial coherent regime but only few in partially coherent even when it is the nature of light. Studies have shown that partially coherent beams have the same applications that their reciprocal scalar beams, but they are more resilient to atmospheric fluctuations. However, the generation and characterization of partially coherent beams are still lacking and even more their vector form. In this thesis we present the mathematical model, the computational generation of the **Partially Coherent Vector Beam (PCVB)** and two experimental setups to generate them with the aid of a Digital Micro Mirror Device (DMD). The expected theoretical results agree with our simulations and pave the way for further theoretical and experimental results, which are left as a future work.

Acknowledgement

It is a pleasure to thank those who supported me along this journey. First of all I would like to thank Professor Carmelo Rosales-Guzman for giving me the opportunity to join his group and for all of his help and support throughout my Master Degree. In you I not only find an admirable scientist but also a great human being. I'm also very grateful to my Structured Light Group colleagues and friends: Dayver Daza, Israel Mecillas, Edgar Medina, Leonardo Culin, Elizabeth Rodriguez for all the laughter and learning in the lab, for teaching me everything they knew and for their patience.

I am heartily thankful to my parents Mirna Soto and Alejandro Arvizu, as well as my brothers Jorge, Alejandra, Aldair, Ricardo and Elias who have always encouraged me to succeed. Thanks to my aunts Diana and Rosa, my uncle Tavito and to all who welcomed me with pleasure every time I returned home.

Thanks to my psychiatrist Melissa Flores Franco for helping me and keeping me alive during this adventure. Along the same lines, I owe my deepest gratitude to Carlos Martinez who has played an essential role during this two years of hard work keeping me alive too. Carlos, you know how much I love you and this Master degree is a shared achievement.

Last but not least, I offer my regards to all of those who supported me in any respect during the completion of my Master Degree: to my teachers who taught me the basis of optics and more, to my classmates, to the laboratory staff who were attentive to all my needs, to the administrative and cleaning staff.

Agradecimientos

Esta tesis no hubiera sido posible sin el apoyo financiero del CONAHCyT.

Es un placer para mí agradecer a quienes me apoyaron en este viaje. En primer lugar me gustaría agradecer al Profesor Carmelo Rosales-Guzmán por darme la oportunidad de unirme a su grupo, por toda su ayuda y apoyo durante mi maestría. En usted no sólo encuentro un científico admirable sino también un gran ser humano. También estoy muy agradecida con mis compañeros y amigos del Grupo de Luz Estructurada: Dayver Daza, Israel Mecillas, Edgar Medina, Leonardo Culin, Elizabeth Rodriguez, gracias por todas las risas y aprendizaje en el laboratorio, por enseñarme todo lo que sabían y por su paciencia.

Agradezco de corazón a mis padres Mirna Soto y Alejandro Arvizu, a mis hermanos Jorge, Alejandra, Aldair, Ricardo y Elías, quienes siempre me han animado a triunfar. A mis tías Rosa, Diana, a mi tío Tavito y a todos los que me recibieron con gusto cada vez que regresaba a casa.

Gracias a mi psiquiatra Melissa Flores Franco por ayudarme y mantenerme con vida durante esta aventura. En la misma línea, debo mi más profundo agradecimiento a Carlos Martínez quien ha jugado un papel esencial durante estos dos años de arduo trabajo para mantenerme con vida también. Carlos, tú sabes cuánto te quiero y que esta maestría es un logro compartido.

Por último, pero no menos importante, ofrezco mi gratitud a todos aquellos que me apoyaron en cualquier aspecto durante la realización de mi Maestría: a mis profesores que me enseñaron las bases de la óptica y más; a mis compañeros, al personal del laboratorio que atendieron todas mis necesidades, al personal administrativo y de limpieza.

To my best friend, Mr. P.

Contributions

Part of the experimental work done in this thesis is reported on a preprint article

"*Generation of super-stable vector modes using on-axis complex-amplitude modulation*"

A colaboration with Valeria Rodriguez-Fajardo, Fernanda Arvizu, Dayver Daza-Salgado, Benjamin Perez-Garcia and Carmelo Rosales-Guzman.

Contents

List of Figures

Acronym list

PCVB Partially Coherent Vector Beam

DMD Digital Micro Mirror Device

PCBs Partially Coherent Beams

SLM Spatial Light Modulator

PCVB Partially Coherent Vector Beam

LG Laguerre-Gaussian

HLG Helical Laguerre-Gaussian

IG Ince-Gaussian

HIG Helical Ince-Gaussian

MG Mathieu-Gaussian

HMG Helical Mathieu Gaussian

PSA Polarization State Analyzer

CCD Charge-Coupled Device

HWP Half-Wave plate retarder

QWP Quarter-Wave plate retarder

LP Linear polarizer

DLP Digital Light Processing

VB Vector Beam

HOPS High Order Poincaré Sphere

HLGVB Helical Laguerre-Gaussian Vector Beam

HIGVB Helical Ince-Gaussian Vector Beam

HMGVB Helical Mathieu-Gaussian Vector Beam

MO Microscope Objective

SF Spatial Filter

PBS Polarizer Beam Splitter

PR Polarization reconstruction

PCHLGVB Partially Coherent Helical Laguerre-Gaussian Vector Beam

PCHIGVB Partially Coherent Helical Ince-Gaussian Vector Beam

PCHMGVB Partially Coherent Helical Mathieu-Gaussian Vector Beam

Introduction

Polarization and coherence are both inherent characteristics of an electromagnetic wave and they are the main focus in this manuscript. Coherence is, in essence, a consequence of correlations between two or more fluctuating electric fields, and there are two types: *temporal* and *spatial*. Temporal coherence refers to the correlation between waves that are observed at two different instants, whilst the spatial coherence describes the correlation between waves at different points in space. The theory of coherence has been extensively explored. In this thesis, we are only to explore the transverse spatial coherence, that is, the correlation between different points of a beam at two different location in space or, in other words, the capability that two separate points in space at the same z-plane have to interfere [1, 2, 3].

Polarization is a remarkable feature of light and it plays a significant role in a variety of applications. Polarization is the manifestation of correlations involving transverse components of the fluctuating electric field at a single point [4, 5]. In 1852, George Stokes defined a mathematic alternative to describe the fully polarized, partially polarized and unpolarized light in terms of its total intensity, degree of polarization and the shape parameters of the polarization ellipse [6]. The degrees of coherence and polarization of light are the fundamental features of any light field and have been treated separately until two decades ago. For many years, the study of the state of polarization of a light beam was assumed invariant as the beam propagates just as an idealized model to simplify the mathematics [5, 4]. The same occurs to the state of polarization and the degree of polarization of partially coherent light but in 1994, James showed that the degree of polarization of a partially coherent beams may in general change on propagation in free space [7]. In 1998, Gori [8] and in 2003, Wolf [9] introduced the unified theory of coherence and polarization for Partially Coherent Beams (PCBs) in time and frequency domains, respectively. They conclude that both properties are interrelated. This knowledge supports the *vector beams* because they refer to those beams in which the spatial mode and polarization cannot be separated.

Efforts have been made on characterization, generation, propagation and detec-

tion of PCBs due to their applications in free-space optical communications, remote sensing, optical imaging, particle trapping, particle scattering, and material thermal processing because it is known that the combination of polarization and partial coherence has led to the discovery of novel effects. For example these kind of beams are more robust toward scintillation caused by atmospheric turbulence [10, 11, 12, 13, 14].

The purpose of this thesis is to present a way to generate partially spatial coherent vector beams by numerical simulation and experimentally. The technique involves the knowledge of some concepts of wave theory, programming, and beam profile measurements. After this Introduction, in Chapter 1 we present the underlying electromagnetic theory and mathematical techniques applicable to structured light. The Helmholtz equation and the approach to its paraxial form are fundamental to arrive at the families of solutions studied in this work. The main concepts of polarization, coherence lead us to the unified theory of polarization and coherence, basis of partially coherent vector beams. DMD and Spatial Light Modulator (SLM) are presented as tools to generate vector beams. In Chapter 2 the generalities about vector beams, how to generate them using two different experimental set-ups and some examples of theoretical and experimental vector beams of the three families mainly studied in this thesis are presented.

Finally, in Chapter 3 my contributions to the are of structured ligh are presented: the generation of partially coherent vector beams. In previous works we can find that there are many ways to generate partially coherent light like using a spiral plate and broadband white light passing through it to generate optical vortices[15], focusing a laser light onto a rotating ground-glass disk and a SLM showing a digital hologram [3, 16, 17, 18] and previous techniques are also noninterferometric [19]. In those techniques controlling the coherence is not a straightforward task because they implies moving optical elements. Our proposal does not involve the movement of any physical element in the experimental set-up because this was migrated to the DMD digitally so that it allows more control of coherence.

Chapter 1

Preliminaries

In this Chapter we describe the basic theory to supports our proposal. In Section 1.1 the derivation of the Helmholtz paraxial wave equation using the wave theory is presented. In Section 1.2 some of the solutions to the Helmholtz equation in different coordinate systems are presented. A brief explanation of polarization, its mathematical description and the techniques to measure it are presented in Section 1.4 while in Section 1.5 coherence is discussed, the other main property studied in this thesis. Finally, in Section 1.6 some of the instruments used to structure light known as spatial light modulators are described.

1.1 Helmholtz paraxial wave equation.

The wave theory postulates that light propagates in the form of waves that can be described by a mathematical function called **wave function** $u(\mathbf{r}, t)$ where $\mathbf{r} = (x, y, z)$ is a real function of position and t is time. This wave function satisfies a partial differential equation called **wave equation**

$$\nabla^2 u - \frac{1}{c^2} \frac{\partial^2 u}{\partial t^2} = 0 \tag{1.1}$$

where ∇^2 is the Laplacian operator in Cartesian coordinates

$$\nabla^2 = \frac{\partial^2}{\partial x^2} + \frac{\partial^2}{\partial y^2} + \frac{\partial^2}{\partial z^2} \tag{1.2}$$

Any function that satisfies 1.1 represents a possible optical wave and, since it is linear, the **principle of superposition** applies: if $u_1(\mathbf{r}, t)$ and $u_2(\mathbf{r}, t)$ represent possible optical waves, then $u(\mathbf{r}, t) = u_1(\mathbf{r}, t) + u_2(\mathbf{r}, t)$ also represents a possible optical wave

[20]. We are going to explore some of the main parameters of the light waves that we are going to use in the future pages of this work.

1.1.1 Some light wave parameters

The optical **intensity** $I(\mathbf{r}, t)$ also called **irradiance** is the optical power per unit area, this means that is transmitted through an imagined surface perpendicular to the propagation direction, the units are $\mathbf{W/m^2}$

$$I(\mathbf{r}, t) = \epsilon_0 c \langle u^2(\mathbf{r}, t) \rangle \tag{1.3}$$

where c is the light speed ($c = 2.9979 \times 10^8 m/s^2$) and ϵ_0 the electric permittivity of free space, ($\epsilon_0 = 8.8542 \times 10^{-12} C^2/N \cdot m^2$). The optical intensity and the **power**, which is going to be explored subsequently, are averaged over at least one oscillation cycle and the operation $\langle . \rangle$ denotes averaging over a time interval. The optical **power** $P(t)$ is the energy per unit time transported by a light wave that is flowing into an area A normal to the direction of propagation of light is the integrated intensity, this means that units are watts, $\mathbf{W}$ [21, 20].

$$P(t) = \int_A I(\mathbf{r}, t) dA \tag{1.4}$$

The optical **energy** E collected in a specific time is the integral of the optical power over this time interval.

$$E(t) = \int P(t) dt \tag{1.5}$$

Now that we know those parameters about light waves, we can continue the analysis.

1.1.2 Hemholtz equation

In order to obtain the Helmholtz equation we must star with the time-independent wave equation. We proposed a well known solution which is a wave function with harmonic time dependence.

$$u(\mathbf{r}, t) = a(\mathbf{r}) \cos[2\pi\nu t + \varphi(\mathbf{r})] \tag{1.6}$$

where $a(\mathbf{r})$ is the amplitude, $\varphi(\mathbf{r})$ is the phase, ν is the frequency ($\mathbf{Hz}$), $\omega = 2\pi\nu$ is the angular frequency ($\mathbf{radians/s}$) and $T = 1/\nu$ is the period ($\mathbf{s}$). As we can see, the amplitude and the phase are both position dependent but the wave function is a

harmonic function of time with frequency ν at all positions.

In a homogeneous medium in regions free of currents and charges, each rectangular component $U(\mathbf{r}, t)$ of the field vectors satisfies the homogeneous wave equation It is very common to represent the real wave function $u(\mathbf{r}, t)$ in eq. 1.6 as a complex function

$$U(\mathbf{r}, t) = a(\mathbf{r}) \exp[j\varphi(\mathbf{r})] \exp(j2\pi\nu t) \tag{1.7}$$

so that

$$u(\mathbf{r}, t) = \mathrm{Re}\{U(\mathbf{r}, t)\} = \frac{1}{2}[U(\mathbf{r}, t) + U^*(\mathbf{r}, t)] \tag{1.8}$$

where the $*$ stands for the complex conjugated. The function $U(\mathbf{r}, t)$ is known as the **complex wave function** and satisfies the wave equation

$$\nabla^2 U - \frac{1}{c^2} \frac{\partial^2 U}{\partial t^2} = 0 \tag{1.9}$$

If we referred $U(\mathbf{r}) = a(\mathbf{r}) \exp[j\varphi(\mathbf{r})]$ as the **complex amplitude** of the wave and, since it is now a separable function, then eq. 1.7 may be rewritten as

$$U(\mathbf{r}, t) = U(\mathbf{r}) \exp(j2\pi\nu t) \tag{1.10}$$

the wave function $u(\mathbf{r}, t)$ is related to the complex amplitude by

$$u(\mathbf{r}, t) = \mathrm{Re}\{U(\mathbf{r}) \exp(j2\pi\nu t)\} = \frac{1}{2}\left[U(\mathbf{r}) \exp(j2\pi\nu t) + U^*(\mathbf{r}) \exp(-j2\pi\nu t)\right] \tag{1.11}$$

Now we can derive the Helmholtz equation by substituting eq. 1.10 into the wave equation eq. 1.9 leads to a differential equation for the complex amplitude $U(\mathbf{r})$

$$\nabla^2 U + k^2 U = 0 \tag{1.12}$$

which is known as the **Helmholtz equation** where

$$k = \frac{2\pi\nu}{c} = \frac{\omega}{c} \tag{1.13}$$

is the **wavenumber**. The Helmholtz equation as we can see throughout its development, describes the propagation of a monochromatic wavelight no paraxial in a uniform space and admits solutions using the separation of variables method generating 14 beams in 4 coordinate systems [20, 22]. The optical intensity of a monochromatic wave can be obtained putting eq. 1.6 into eq. 1.3.

$$I(\mathbf{r}, t) = 2a^2(\mathbf{r}) \cos^2[2\pi\nu t + \varphi(\mathbf{r})]$$
$$= |U(\mathbf{r})|^2 \{1 + \cos(2[2\pi\nu t + \varphi(\mathbf{r})])\} \tag{1.14}$$

If we average the last expression over a time longer than an optical period, $T = 1/\nu$ vanishes the second term

$$I(\mathbf{r}) = |U(\mathbf{r})|^2 \tag{1.15}$$

This means that, theoretically, the intensity of a monochromatic wave does not vary with time.

1.1.3 Elementary waves

The plane wave

The plane wave has a complex amplitude

$$U(\mathbf{r}) = A \exp(-j\mathbf{k} \cdot \mathbf{r}) = A \exp[-j(k_x x + k_y y + k_z z)] \tag{1.16}$$

where A is the **complex envelope** that represents the strenght of the wave and $\mathbf{k} = (k_x, k_y, k_z)$ is the **wavevector**. Substituting eq. 1.16 into Helmholtz equation, eq. 1.12

$$\nabla^2 U + (k_x^2 + k_y^2 + k_z^2)U = 0 \tag{1.17}$$

yields the relation $(k_x^2 + k_y^2 + k_z^2) = k^2$ so that the magnitude of the wavevector $\mathbf{k}$ is the wavenumber k. Since the phase of the wave is $\arg\{U(\mathbf{r})\} = \arg\{A\} - \mathbf{k} \cdot \mathbf{r}$. Neglecting the constant phase term $\arg\{A\}$, the surfaces of constant phase (wavefronts) obey $\mathbf{k} \cdot \mathbf{r} = k_x x + k_y y + k_z z = 2\pi q$ with q integer. This is the equation describing parallel planes perpendicular to the wavevector $\mathbf{k}$. Consecutive planes are separated by a distance $\lambda = 2\pi/k$ so that

$$\lambda = \frac{c}{\nu} \tag{1.18}$$

where λ is called **wavelength**. The plane wave has a constant intensity $I(\mathbf{r}) = |A|^2$ everywhere in space so that it carries infinite power. This is clearly an idealization since it exist everywhere and at all times. If a monochromatic wave propagates through media of different refractive indices, its frequency will remains the same but its velocity, wavelength and wavenumber will be altered

$$c = \frac{c_0}{n}, \lambda = \frac{\lambda_0}{n}, k = nk_0 \tag{1.19}$$

A wave is said to be paraxial if its wavefront normals are paraxial rays, in this way, we can construct a paraxial wave of a plane wave which is propagating parallel to z-axis using eq. 1.16

$$U(\mathbf{r}) = A(\mathbf{r})\exp(-jkz) \tag{1.20}$$

The paraxial waves

To satisfy the Helmholtz equation for the paraxial wave, the complex envelope $A(\mathbf{r})$ must satisfy another partial differential equation that is obtained by substituting eq. 1.20 into eq. 1.12. Here it is important to take some important assumptions, $A(r)$ varies very slow with respect to z which means that a distance $\Delta z = \lambda$, the change ΔA is much smaller than A itself.

$$\Delta A = \left(\frac{\partial A}{\partial z}\right)\Delta z = \left(\frac{\partial A}{\partial z}\right)\lambda$$
$$\therefore \frac{\partial A}{\partial z} \ll \frac{A}{\lambda} = \frac{Ak}{2\pi} \tag{1.21}$$
$$\frac{\partial A}{\partial z} \ll kA$$

The derivative $\partial A/\partial z$ also vary slowly within the distance λ so

$$\frac{\partial^2 A}{\partial z^2} \ll k\frac{\partial A}{\partial z} \tag{1.22a}$$

$$\frac{\partial^2 A}{\partial z^2} \ll k^2 A \tag{1.22b}$$

using eq. 1.20 into eq. 1.12

$$\nabla^2 U + k^2 U = 0 \tag{1.23a}$$

$$A(\mathbf{r})\exp(-jkz)\frac{\partial^2 A}{\partial x^2} + A(\mathbf{r})\exp(-jkz)\frac{\partial^2 A}{\partial y^2} + A(\mathbf{r})\exp(-jkz)\frac{\partial^2 A}{\partial z^2}... \tag{1.23b}$$

$$+k^2 A(\mathbf{r})\exp(-jkz) = 0 \tag{1.23c}$$

$$\tag{1.23d}$$

Neglecting $\partial^2 A/\partial z^2$ in comparison with $k\partial A/\partial z$ or $k^2 A$,

$$\nabla_T^2 A - j2k\frac{\partial A}{\partial z} = 0 \tag{1.24}$$

where $\nabla_T^2 = \partial^2/\partial x^2 + \partial^2/\partial y^2$ is the transverse Laplacian operator. This equation is called **paraxial Helmholtz equation**. This equation has multiple solutions for dif-

ferent coordinate systems, for example, **Laguerre-, Ince-** and **Mathieu-Gaussian** modes.

1.2   Solutions to the Helmholtz equation

1.2.1   Laguerre-Gaussian Modes

The **Laguerre-Gaussian (LG)** modes are a complete set of exact solution to the paraxial Helmholtz equation in cylindrical coordinates (ρ, ϕ, z)

$$\left(\frac{1}{\rho} \frac{\partial}{\partial \rho} \left(\rho \frac{\partial}{\partial \rho} \right) + \frac{1}{\rho^2} \frac{\partial^2}{\partial \phi^2} - 2ik \frac{\partial}{\partial z} \right) u(\rho, \phi, z) = 0 \tag{1.25}$$

and using separation-of-variable technique in ρ and ϕ, the complex amplitude of the LG beam, LG_{lm} can be expressed as [20]

$$\mathrm{LG}_{l,m}^{e,o}(\rho, \phi, z) = A_{l,m} \left[\frac{W_0}{W(z)} \right] \binom{\cos l\phi}{\sin l\phi} \left(\frac{\rho}{W(z)} \right)^l \mathbb{L}_m^l \left(\frac{2\rho^2}{W^2(z)} \right) \exp \left(-\frac{\rho^2}{W^2(z)} \right) \ldots$$
$$\ldots \exp \left[-jkz - jk\frac{\rho}{2R(z)} \mp jl\phi + j(l + 2m + 1)\zeta(z) \right] \tag{1.26}$$

where the $\mathbb{L}_m^l(\cdot)$ represent generalized Laguerre polynomials and $W(z), R(z), \zeta(z)$ and W_0 are given by

$$W(z) = W_0 \sqrt{1 + \left(\frac{z}{z_0} \right)^2} \tag{1.27a}$$

$$R(z) = z \left[1 + \left(\frac{z_0}{z} \right)^2 \right] \tag{1.27b}$$

$$\zeta(z) = \arctan \frac{z}{z_0} \tag{1.27c}$$

$$W_0 = \sqrt{\frac{\lambda z_0}{\pi}} \tag{1.27d}$$

Here

$$\mathbb{L}_m^l(x) = (m + l)! \sum_{i=0}^{m} \frac{(-x)^i}{i!(m - i)!(l + i)!} \tag{1.28}$$

are the generalized Laguerre polynomials. The set of beams of complex amplitude generated by the eq. 1.26 are known as **Laguerre-Gaussian Beams** even (e) and odd (o) due to the cosine and sine functions in the solution. The integers $l = 0, 1, 2, \ldots$ and $m = 0, 1, 2, \ldots$ are azimuthal and radial indices. The LG modes are optical vortices
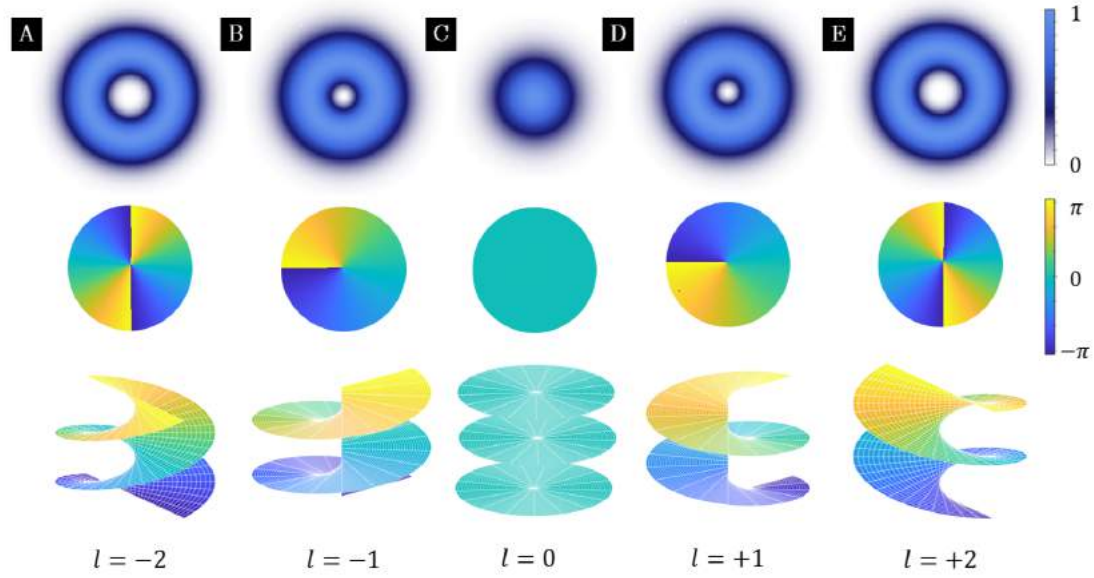
Figure 1.1: Helical Laguerre-Gaussian modes with different value of l. Some transverse intensities and phase distributions with the characteristic wavefront which is a helical surface A) LG$(-2, 0)$, B) LG$(-1, 0)$, C) LG$(0, 0)$, or gaussian mode, D) LG$(1, 0)$ and E) LG$(2, 0)$.

due to the helical phase $\exp(jl\phi)$ which change with the azimuthal angle ϕ along the optical axis. This dependence on ϕ results in a spiraling phase front, while the intensity pattern will always show unbroken concentric rings. These modes are also called **Helical Laguerre-Gaussian (HLG)** modes because of their phase structure [23]. This properties can be observed in Figure 1.1 where we have some transverse intensity distributions that take the form of a toroid because it is proportional to the absolute square of eq. 1.26 which is a function of ρ, z but not of ϕ, so that is azimuthally symmetric. The number of torsion that a LG mode can have over a wavelength λ received the name of topological charge (l) and it takes positive and negative numbers. In Figure 1.1 we can see that beams with $l \neq 0$ have zero intensity at the beam center and with $l = 0$, we obtain a Gaussian fundamental mode. In the phase distribution is important to remark how the direction of rotation changes with the sign of l and this is more obvious with the wavefront graphic where the helical behavior is evident all this while the intensity distribution remains the same. The number number of rings in a LG mode is given by the relation $(m + 1)$ for $m \neq 0$. This can be clearly seen in Figure 1.2 where the parameter m is changing and how multiple rings are added.
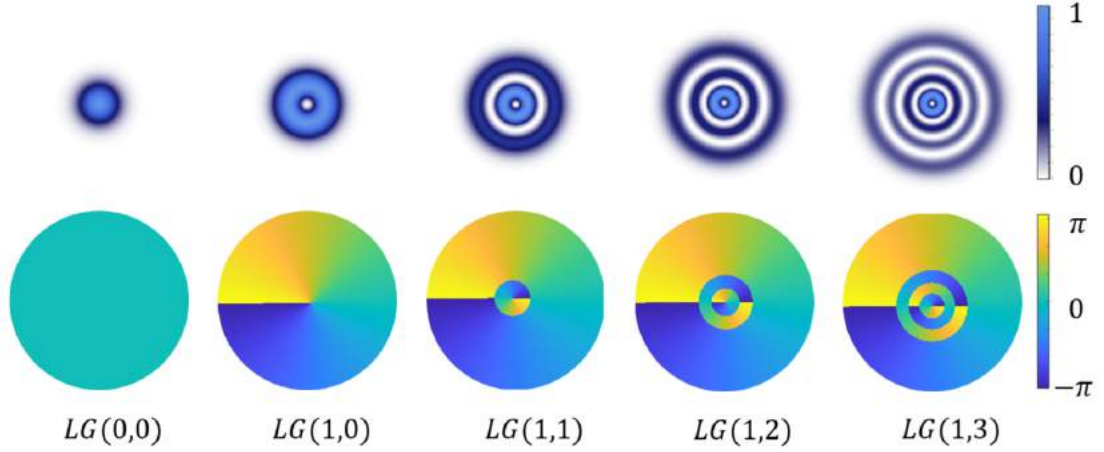
Figure 1.2: Laguerre Gaussian modes with different value of m. Transverse intensity (top) and phase (bottom) distributions.

1.2.2   Ince-Gaussian Modes

The **Ince-Gaussian (IG)** modes are a complete set of exact solutions in elliptic coordinates to the paraxial Helmholtz equation. The complex amplitude of these beams is characterized by Ince polynomials. The paraxial Helmholtz equation in elliptic coordinates is given by

$$\frac{1}{f^2(\cosh^2 \epsilon - \cos^2 \eta)}\left[\frac{\partial^2 \Psi(\mathbf{r})}{\partial \xi^2} + \frac{\partial^2 \Psi(\mathbf{r})}{\partial \eta^2}\right] + 2ik\frac{\partial \Psi(\mathbf{r})}{\partial z} = 0 \qquad (1.29)$$

where $f(z) = f_0 W(z)/W_0$ is the semi-focal distance (eccentricity) of the coordinate system with f_0 as the initial separation in $z = 0$. The solution of the paraxial Helmholtz equation is a pair of beams modulated by an gaussian envelope known as Ince-Gaussian modes given by

$$IG^e_{p,m;\epsilon}(\mathbf{r}) = \mathcal{C}\frac{W_0}{W(z)}C^m_p(\imath\xi;\epsilon)C^m_p(\eta;\epsilon)\exp\left\{\left[\frac{-\rho^2}{W^2(z)}\right]\right\} \times \cdots$$
$$\cdots \times \exp\left[\imath\left(kz + \frac{k\rho^2}{2R(z)} - (p+1)\zeta(z)\right)\right] \qquad (1.30)$$

$$IG^o_{p,m;\epsilon}(\mathbf{r}) = \mathcal{S}\frac{W_0}{W(z)}S^m_p(\imath\xi;\epsilon)S^m_p(\eta;\epsilon)\exp\left\{\left[\frac{-\rho^2}{W^2(z)}\right]\right\} \times \cdots$$
$$\cdots \times \exp\left\{\left[\imath\left(kz + \frac{k\rho^2}{2R(z)} - (p+1)\zeta(z)\right)\right]\right\}, \qquad (1.31)$$

where C_p^m and S_p^m are the even and odd Ince polynomials with $0 \leq m \leq p$ to even functions and $1 \leq m \leq p$ to odd function; the indices p, m always have the same parity, p indicates the order and m the degree and C and S are normalization constants. The complex amplitude of the Ince-Gaussian beam, IG_{pm}^e can be expressed as

$$U_{p,m}^e(\rho, phi, z) = \mathcal{D}^2 \frac{W_0^2}{W^2(z)} [D_m^n(i\xi; \epsilon)]^2 [D_m^n(\eta; \epsilon)]^2 \exp\left[\frac{-2\rho^2}{W^2(z)}\right] \tag{1.32}$$

where $\mathcal{D}$ can be C or S depending on whether the solution is even or odd, respectively. The Laguerre-Gaussian and Hermite-Gaussian are limiting forms of IG beams when the ellipticity parameter is 0 and ∞, respectively [20, 24].

Helical Ince-Gaussian Modes.

The **Helical Ince-Gaussian (HIG)** modes are built by a linear combination of the even and odd IG beams [25, 26]

$$\mathrm{HIG}_{p,m,e}^+(\xi, \eta) = \mathrm{IG}_{p,m,\epsilon}^e(\xi, \eta, \epsilon) + i\mathrm{IG}_{p,m,\epsilon}^o(\xi, \eta, \epsilon) \tag{1.33a}$$

$$\mathrm{HIG}_{p,m,e}^-(\xi, \eta) = \mathrm{IG}_{p,m,\epsilon}^e(\xi, \eta, \epsilon) - i\mathrm{IG}_{p,m,\epsilon}^o(\xi, \eta, \epsilon) \tag{1.33b}$$

where $m > 0$ because $\mathrm{IG}_{p,m,\epsilon}^o$ is not defined for $m = 0$.

1.2.3 Mathieu-Gaussian Modes

The **Mathieu-Gaussian (MG)** modes are a set of solution of the Helmholtz equation in elliptical cylindrical coordinates where the solution are divided in two functions, one of them longitudinal and the other, transversal. The cartesian cordinates (x, y, z) are related to the elliptical coordinates (ξ, η, z) as $(x = f \cosh \xi \cos \eta)$ and $(y = \sinh \xi \sin \eta)$ and $(z = z)$. The Helmholtz equation in elliptical cylindrical coordinates is given by

$$\frac{\partial^2 U}{\partial \xi^2} + \frac{\partial^2 U}{\partial \eta^2} + \frac{f^2 k_t^2}{2}(\cosh 2\xi - \cos 2\eta)U = 0 \tag{1.34}$$

where $U(\xi, \eta)$. In this coordinates, $\xi \in [0, \infty)$ is the radial coordinate, $\eta \in [0, 2\pi)$ is the angular coordinate and $z \in (-\infty, \infty)$ is the propagation one. The major and minor axis, a and b, respectively, defines the parameter f which is the semi-focal distance $f^2 = a^2 - b^2$ and is related to the eccentricity e by $e = f/a$. The wave vector $\mathbf{k}$ satisfies the relation $k^2 = k_t^2 + k_z^2$ where k_t and k_z are the transverse and

the longitudinal components of the wave vector respectively. The solutions of the eq. 1.34 are the radial and angular Mathieu functions

$$\text{M}^{\text{e}}_{\text{m}}(\xi, \eta; q) = C_m \text{Je}(\xi, q)\text{ce}_m(\eta, q) \tag{1.35a}$$

$$\text{M}^{\text{o}}_{\text{m}}(\xi, \eta; q) = S_m \text{Jo}(\xi, q)\text{se}_m(\eta, q) \tag{1.35b}$$

where C_m and S_m are normalization constants. The angular even and odd Mathieu function are ce_{m} and se_{m} respectively where the sub-index m indicates the order of the function, $m = 0, 1, 2, 3...$ for even modes and $m = 1, 2, 3, ...$ for odd modes. The $mth-$order functions Je_{m} and Jo_{m} are even and odd radial Mathieu functions. The modes described by the eq. 1.35 are the non-diffracting Mathieu beams, this means that carry an infinite amount of energy and cannot be realised experimentally. To avoid the infinite energy, we can introduce a gaussian envelope to generate MG beams which retain the non-diffracting properties over a finite propagation distance.

$$\text{MG}^{\text{e}}_{\text{m}}(\tilde{\xi}, \tilde{\eta}, z; q) = \exp\left(-\frac{ik_t^2}{2k}\frac{z}{\mu}\right)\text{GB}(\mathbf{r})\text{M}^{\text{e}}_{\text{m}}(\tilde{\xi}, \tilde{\eta}; q), \tag{1.36a}$$

$$\text{MG}^{\text{o}}_{\text{m}}(\tilde{\xi}, \tilde{\eta}, z; q) = \exp\left(-\frac{ik_t^2}{2k}\frac{z}{\mu}\right)\text{GB}(\mathbf{r})\text{M}^{\text{o}}_{\text{m}}(\tilde{\xi}, \tilde{\eta}; q), \tag{1.36b}$$

where the Cartesian coordinates (x, y) are redefined in terms of the complex elliptic variables (ξ, η) as $x = f_0(1 + iz/z_R)\cosh\bar{\xi}\cos\bar{\eta}$ and $y = f_0(1 + iz/z_R\sinh\bar{\xi}\sin\bar{\eta})$ with f_0 the semi-focal distance at z=0 and $\mathbf{GB}(\mathbf{r})$ is the fundamental Gaussian beam defined as

$$\mathbf{GB}(\mathbf{r}) = \exp\left(-\frac{r^2}{\mu\omega_0^2}\right)\frac{\exp(ikz)}{\mu} \tag{1.37}$$

The parameter $\mu = \mu(z)$ is defined as $\mu = 1 + iz/z_R$ with $z_R = k\omega_0^2$ being the Rayleigh range of a Gaussian beam with waist radius ω_0 [27].

Helical Mathieu-Gaussian modes

The Helical Mathieu Gaussian (HMG) modes can be obtained by a linear combination given by the odd and even modes

$$\text{HMG}^+_m(\tilde{\xi}, \tilde{\eta}, z; q) = \text{MG}^e_m(\tilde{\xi}, \tilde{\eta}, z; q) + i\text{MG}^o_m(\tilde{\xi}, \tilde{\eta}, z; q) \tag{1.38a}$$

$$\text{HMG}^-_m(\tilde{\xi}, \tilde{\eta}, z; q) = \text{MG}^e_m(\tilde{\xi}, \tilde{\eta}, z; q) - i\text{MG}^o_m(\tilde{\xi}, \tilde{\eta}, z; q) \tag{1.38b}$$

1.3   Interference of Light

Optical interference corresponds to the superposition of two or more individual waves that, under certain conditions produce a resultant irradiance pattern, known commonly as an interference pattern, that deviates from the sum of the irradiances of the individual waves.

$$I(\mathbf{r},t) \neq \sum_i I_i(\mathbf{r},t), \tag{1.39}$$

The necessary conditions for a well-defined interference pattern are that the waves have the same or nearly the same wavelength, the amplitudes of the waves must be the same or nearly equal and they must be in phase with each other and propagate in the same homogeneous medium in the same direction or with a very small angle. For polarized light, the interfering waves must have the same state of polarization. The first conditions can be achieved if the interacting waves originate from the same monochromatic source and with this, it can also be ensured that the interference pattern of maximums and minimums will be stationary. If the source is polychromatic, such as white light, then the different interference patterns produced by the interaction between waves of the same wavelength will overlap each other. On the other hand, if the waves travel at very large angles before interacting with each other, the interference phenomenon will still be present. However, the space between the bright and dark fringes will be small so the fringes may become indistinguishable [1, 28, 29].

Let's assume a monochromatic linearly polarized emitting source from which, by two holes separated by a distance a much greater than the wavelength λ, two point sources S_1 and S_2 are obtained and they propagate in a homogeneous medium. On an observation plane that is far enough away so that the wavefronts of the waves are planes, point P is located as shown in Figure 1.3. The waves have the form of eq. 1.6.

$$\mathbf{u}_1(\mathbf{r},t) = \mathbf{a}_1(\mathbf{r}) \cos[\mathbf{k_1} \cdot \mathbf{r} - \omega t + \phi_1] \tag{1.40a}$$

$$\mathbf{u}_2(\mathbf{r},t) = \mathbf{a}_2(\mathbf{r}) \cos[\mathbf{k_2} \cdot \mathbf{r} - \omega t + \phi_2] \tag{1.40b}$$

The irradiance is given by eq. 1.3 so, then we have

$$I = \epsilon_0 c \langle \mathbf{u}_1 \cdot \mathbf{u}_2 \rangle \tag{1.41}$$

We are going to neglect the constants since we are concerned only with relative
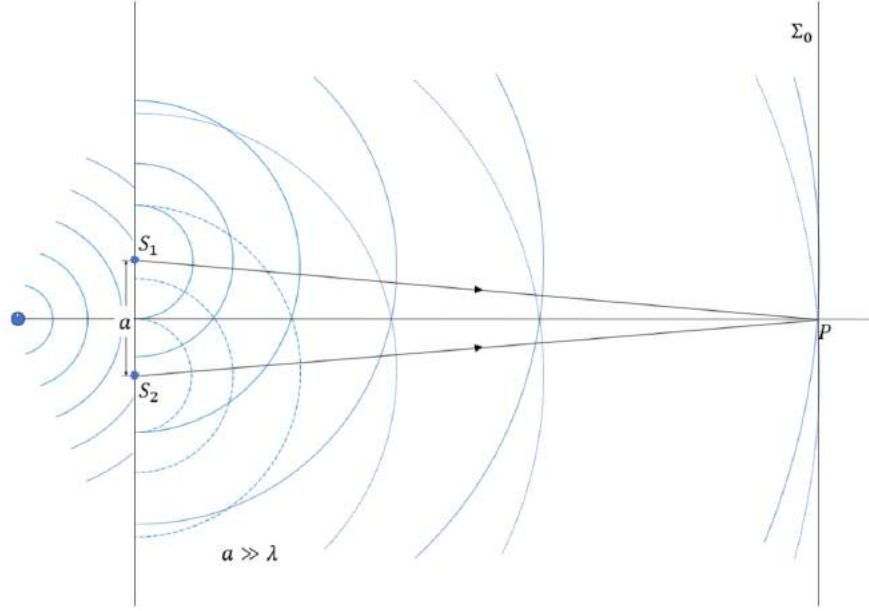
Figure 1.3: Waves from two point sources, S_1 and S_2 separated by a distance a overlapping in space at point P.

irradiances. Thus the irradiance at P is given by

$$I = \langle \mathbf{u}_1^2 + \mathbf{u}_2^2 + 2\mathbf{u}_1\mathbf{u}_2 \rangle \tag{1.42}$$

In eq. 1.42, the first two terms corresponds to the irradiances of the individual waves, I_1 and I_2. The last term is the result of the interaction of the waves and is called **interference term**, I_{12}. Then, eq. 1.42 may be written as

$$I = I_1 + I_2 + I_{12} \tag{1.43}$$

The presence of the interference term is due to the wave behaviour of light and it can produces enhancement or diminution of the irradiance through interference [29]. When the wavefields are orthogonal, then the dot product vanishes so there is not interference results but when the wavefields are parallel, the interference term is maximum. Consider the interference term

$$I_{12} = 2\langle \mathbf{u}_1 \cdot \mathbf{u}_2 \rangle \tag{1.44a}$$
$$= 2\langle a_1(\mathbf{r}) \cdot a_2(\mathbf{r}) \cos[\mathbf{k_1} \cdot \mathbf{r} - \omega t + \phi_1] \times \cos[\mathbf{k_2} \cdot \mathbf{r} - \omega t + \phi_2] \rangle \tag{1.44b}$$

and it can be simplified using trigonometric identity $2\cos(A)\cos(B) = \cos(A+B) +$

$\cos(B - A)$. We define $\alpha = \mathbf{k_1} \cdot \mathbf{r} + \phi_1$ and $\beta = \mathbf{k_2} \cdot \mathbf{r} + \phi_2$.

$$I_{12} = 2a_1(\mathbf{r}) \cdot a_2(\mathbf{r}) \cos(\alpha - \omega t) \times \cos(\beta - \omega) \tag{1.45a}$$

$$= 2a_1(\mathbf{r}) \cdot a_2(\mathbf{r})[\langle \cos(\alpha + \beta - 2\omega t)\rangle + \langle \cos(\beta - \alpha)\rangle] \tag{1.45b}$$

The first time average in this relation is taken over a rapidly oscillating cosine function and so is zero. Thus

$$I_{12} = 2a_1(\mathbf{r}) \cdot a_2(\mathbf{r})\langle \cos(\beta - \alpha)\rangle \tag{1.46a}$$

$$= 2a_1(\mathbf{r}) \cdot a_2(\mathbf{r})\langle \cos \delta \rangle \tag{1.46b}$$

where $\delta = \mathbf{k_2} \cdot \mathbf{r} - \mathbf{k_1} \cdot \mathbf{r} + \phi_2 - \phi_1$ is the phase difference arising from a combined path lenght and initial phase-angle difference. For purely monochromatic fields, δ is time-dependent, in which case $\langle \cos \delta \rangle = \cos \delta$. The eq. 1.42 can be written in a more convenient way by noticing that

$$I_1 = \langle \mathbf{u}_1^2 \rangle = \frac{1}{2}a_1(\mathbf{r})^2 \tag{1.47a}$$

$$I_2 = \langle \mathbf{u}_2^2 \rangle = \frac{1}{2}a_2(\mathbf{r})^2 \tag{1.47b}$$

The interference term becomes

$$I_{12} = 2\sqrt{I_1 I_2}\langle \cos \delta \rangle \tag{1.48}$$

and eq. 1.42 is

$$I = I_1 + I_2 + 2\sqrt{I_1 + I_2}\langle \cos \delta \rangle \tag{1.49}$$

1.3.1   Interference of mutually incoherent fields

In practice, $\mathbf{u}_1$ and $\mathbf{u}_2$ are not originated from the same source, this implies that the time average in eq. 1.49 is zero since no source is perfectly monochromatic. For real sources, we must allow the phases ϕ_1 and ϕ_2 to be functions of time. The interference term I_{12} takes the form

$$I_{12} = 2\sqrt{I_1 I_2}\langle cos(\mathbf{k_2} \cdot \mathbf{r} - \mathbf{k_1} \cdot \mathbf{r} + \phi_2(t) - \phi_1(t))\rangle \tag{1.50}$$

The time average in the preceding relation will be zero unless for laser sources with state-of-the-art frequency stability [1, 29]. In such case, the sources are mutually

incoherent and the detected irradiance will be

$$I = I_1 + I_2 \tag{1.51}$$

It is often said, that light beams from independent sources, even if both sources are the same kind of laser, do not interfere with each other. In fact, these fields do interfere but the interference term averages to zero over the averaging times of most real detectors [29].

1.3.2 Interference of mutually coherent fields

If light of the same source is split and then recombined at a detector, the time average in eq. 1.49 need not be zero. Since both waves are from the same source, they are correlated. The phases ϕ_1 and ϕ_2 are equal in magnitude if the waves travel paths of equal duration before being recombined so the interference term takes the form [29],

$$I_{12} = 2\sqrt{I_1 I_2} \langle cos(\mathbf{k}_2 \cdot \mathbf{r} - \mathbf{k}_1 \cdot \mathbf{r}) \rangle \tag{1.52a}$$

$$= 2\sqrt{I_1 I_2} \cos(\mathbf{k}_2 \cdot \mathbf{r} - \mathbf{k}_1 \cdot \mathbf{r}) \tag{1.52b}$$

Even if the waves travel different paths that differ in duration by a time δt, the phase difference from the departure from monochromaticity $\phi_2(t) - \phi_1(t + \delta t)$ will be zero o nearly zero so long as δt is less than the **coherence time**, τ_0, of the source which is the time interval where the departures from monochromaticity are small and negligible. We have also the **coherence length** which is the distance that the electric field travels in a coherence time $l_c = c\tau_0$. The coherence length in sources like lasers is from centimeters to kilometers. The concept of coherence will be soon studied. For waves generated by the same source, the difference between the paths of the interferring waves is much smaller than the coherence length. The interference is given by

$$I = I_1 + I_2 + 2\sqrt{I_1 I_2} \cos \delta \tag{1.53}$$

The fields that satisfies the equation above are said to be mutually coherent. At various points in space, the resultant irradiance can be greater, less than, or equal to $I_1 I_2$ that is depending on δ. The maximum irradiance is obtained when $\cos \delta = 1$ that implies $\delta = 0, \pm 2\pi, \pm 4\pi, ..., 2m\pi$ where m is any integer. This phenomena is also called **total constructive interference**

$$I_{max} = I_1 + I_2 + 2\sqrt{I_1 I_2} \tag{1.54}$$
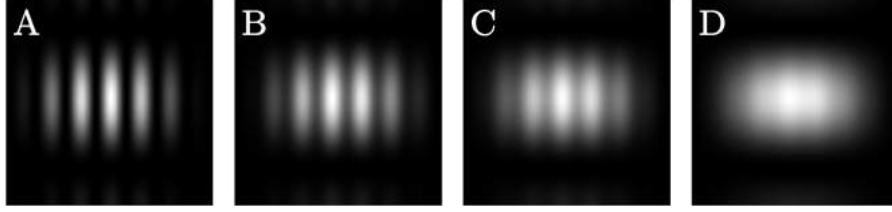
Figure 1.4: Simulation of the interference pattern of a double slit experiment with different Gaussian sources. A) High coherent interference: we can see a sharpness interference pattern, B) and C) partially coherent interference: the interference pattern is blurry, and D) incoherent interference: the interference pattern is null.

We have constructive interference when $0 < \cos\delta < 1$, and $I_1 + I_2 < I < I_{max}$. At $\delta = \pi/2$, $\cos\delta = 0$ which means that the optical waves are $90\,\mathrm{deg}$ out-of-phase, and $I = I_1 + I_2$. The minimum irradiance, also known as **total destructive interference** results when the waves are $180\,\mathrm{deg}$ out-of-phase, troughs overlap crest, $\cos\delta = -1$, this means that $\delta = \pm\pi, \pm3\pi, \pm5\pi, ..., 2(m+1)\pi$

$$I_{min} = I_1 + I_2 - 2\sqrt{I_1 I_2} \tag{1.55}$$

The destructive interference occurs for $-1 < \cos\delta < 0$, and $I_{min} < I < I_1 + I_2$. If both waves have the same amplitude, then $I_{max} = 4I_0$ and $I_{min} = 0$.

The visibility of the interference pattern between of two monochromatic waves of equal amplitudes have 0 as minimum interference and 1 as maximum value. The visibility is given by

$$\text{visibility} = \frac{I_{max} - I_{min}}{I_{max} + I_{min}} \tag{1.56}$$

In Figure 1.4 are shown some examples of interference patterns with different visibility. In Section 1.5, coherence will be detailed but basically the fringes are expected to be very sharp for a spatially coherent source and, as coherence is lost, these fringes will soften and little by little they will disappear until they lost.

1.3.3 Interference and polarization: Fresnel-Arago Laws

Previously it was assumed that the two overlapping optical vector waves were linearly polarized and parallel and the experiment was easy but when the interfering waves have different states of polarization, we need to add this condition to the analysis. Fresnel and Arago studied the phenomena of interference with different states of polarization and conclude their work with four useful laws known as **Fresnel-Arago laws**:

1. Two parallel, coherent linear polarized waves can interfere.

2. Two orthogonal, coherent linearly polarized waves cannot interfere in the sense that $I_{12} = 0$ and no fringe pattern result.

3. Two waves, linearly polarized with orthogonal polarizations, if derived from perpendicular components of unpolarized light and subsequently brought into the same plane, cannot interfere to form a readily observable fringe pattern because these orthogonal polarizations are mutually incoherent.

4. Two waves, linearly polarized with orthogonal polarizations, if derived from the same linearly polarized wave and subsequently brought into the same plane, can interfere.

To appreciate easily the laws, we are going to suppose, for the moment and cover it in the next Section, that any polarization state can be synthesized out of two orthogonal linear polarized states. For example, $\mathbf{u}_\parallel$ and $\mathbf{u}_\perp$ are orthogonal states of polarization so any plane wave, whether polarized or not, can be written as $(\mathbf{u}_\parallel + \mathbf{u}_\perp)$. So the analysis can be start with a wave $(\mathbf{u}_{\parallel 1} + \mathbf{u}_{\perp 1})$ and $(\mathbf{u}_{\parallel 2} + \mathbf{u}_{\perp 2})$ emitted from two identical coherent sources superimpose in some region of space. The resulting flux-density distribution will consist of two independent, precisely overlapping interference patterns $\langle(\mathbf{u}_{\parallel 1} + \mathbf{u}_{\parallel 2})^2\rangle$ and $\langle(\mathbf{u}_{\perp 1} + \mathbf{u}_{\perp 2})^2\rangle$. Even though $\mathbf{u}_{\perp 1}$ and $\mathbf{u}_{\perp 2}$ are parallel to each other, $\mathbf{u}_{\parallel 1}$ and $\mathbf{u}_{\parallel 2}$, which are in the reference plane, need not be and they will be parallel only when $\mathbf{k}_1 = \mathbf{k}_2$ [1, 29, 30].

1.4   Polarization

The state of **polarization** is one of the properties of the light associated to its wave behavior because it is the result of the oscillations of the electric field. Basically, the polarization describes the vector nature of light and refers to the variation in time of the direction of the electric field $\mathbf{E}(\mathbf{r}, t)$ in a determined point $\mathbf{r}$ in the perpendicular plane to wave propagation. Mathematically, the electric wave $\mathbf{E}(z, t)$ can be represented as

$$E_x(z, t) = E_{0x} \cos\left(\omega t - kz - \delta_x(t)\right)\hat{\mathbf{x}} \tag{1.57a}$$

$$E_y(z, t) = E_{0y} \cos\left(\omega t - kz - \delta_y(t)\right)\hat{\mathbf{y}} \tag{1.57b}$$

where E_{0x}, E_{0y} are the amplitudes, both with the same angular frequency ω , k is the wavenumber, z is the direction of propagation and δ_x, δ_y are arbitrary phases. Those components are perpendicular between them and propagates in $z-$ direction. A simple way to describe the polarization of light is the Jones vectors, which are two element complex vectors that describe the polarization states of light through its amplitude and phase

$$\mathbf{J}(t) = \begin{pmatrix} E_x(z,t) \\ E_y(z,t) \end{pmatrix} \tag{1.58}$$

We can write the eq. 1.57 in a complex way and if we suppressed the propagator $\tau = \omega t - kz$, then

$$E_x(z,t) = E_{0x}\exp(i\delta_x) \tag{1.59a}$$

$$E_y(z,t) = E_{0y}\exp(i\delta_y) \tag{1.59b}$$

These two equations can be arranged in a 2×1 column matrix $\mathbf{E}$ so that

$$\mathbf{E} = \begin{pmatrix} E_x(z,t) \\ E_y(z,t) \end{pmatrix} = \begin{pmatrix} E_{0x}\exp(i\delta_x) \\ E_{0y}\exp(i\delta_y) \end{pmatrix} \tag{1.60}$$

To normalize the Jones vector we can use that the total intensity can be obtained by eq. 1.3. In our construction this is

$$I = E_x E_x^* + E_y Ey^* \tag{1.61}$$

This expression can also be obtained by the multiplication of two vectors expressed as

$$I = \begin{pmatrix} E_x^* & E_y^* \end{pmatrix} \begin{pmatrix} E_x \\ E_y \end{pmatrix} = E_{0x}^2 + E_{0y}^2 = E_0^2 \tag{1.62}$$

If we define the row matrix $\begin{pmatrix} E_x^* & E_y^* \end{pmatrix}$ as the complex conjugate transpose $\mathbf{E}^\dagger$ of the Jones vector $\mathbf{E}$ so we have

$$I = \mathbf{E}^\dagger \cdot \mathbf{E} \tag{1.63}$$

It is customary to set $E_0^2 = 1$, so we can say that the Jones vector is normalized

$$\mathbf{E}^\dagger \cdot \mathbf{E} = 1 \tag{1.64}$$

Here is important to say that the Jones vector can **only** be used to describe completely polarized light.

1.4.1 Jones vectors of typical polarized light

Using the Jones vectors is possible to describe the states of polarization of light. For example, to describe the horizontal polarized light, we have that $E_y = 0$ so we can rewrite eq. 1.60 as

$$\mathbf{E} = \begin{pmatrix} E_{0x} \exp(i\delta_x) \\ 0 \end{pmatrix} \tag{1.65}$$

Considering the normalization of the electric field, we have that $E_{0x}^2 = 1$ and due to $\exp(i\delta_x)$ is unimodular, the normalized Jones vector is

$$\mathbf{E} = \begin{pmatrix} 1 \\ 0 \end{pmatrix} \tag{1.66}$$

In a similar way. for the vertical polarized light we have that $E_x = 0$ this means that $E_{0y}^2 = 1$, so we have

$$\mathbf{E} = \begin{pmatrix} 0 \\ 1 \end{pmatrix} \tag{1.67}$$

The light polarized at $+45°$ implies that $E_x = E_y$, then $2E_{0x}^2 = 1$ so we obtain

$$\mathbf{E} = \frac{\sqrt{2}}{2} \begin{pmatrix} 1 \\ 1 \end{pmatrix} \tag{1.68}$$

The same occurs with light polarized at $-45°$ where $E_x = -E_y$ so $2E_{0x}^2 = 1$, the normalized Jones vector is

$$\mathbf{E} = \frac{\sqrt{2}}{2} \begin{pmatrix} 1 \\ -1 \end{pmatrix} \tag{1.69}$$

For the case of right-hand circularly polarized light, $E_{0x} = E_{0y}$ and $\delta_y - \delta_x = +90°$, then $2E_{0x}^2 = 1$ and we have

$$\mathbf{E} = \frac{\sqrt{2}}{2} \begin{pmatrix} 1 \\ i \end{pmatrix} \tag{1.70}$$

Left-hand circularly polarized light has $E_{0x} = E_{0y}$ and $\delta_y - \delta_x = -90°$. The normalization conditions gives $2E_{0x}^2 = 1$ and we obtain

$$\mathbf{E} = \frac{\sqrt{2}}{2} \begin{pmatrix} 1 \\ -i \end{pmatrix} \tag{1.71}$$

1.4.2 Polarization ellipse

The polarization ellipse is a way to visualize the polarization state. To construct this representation we use the arguments described previously and summarized in eqs. 1.57 where the propagator $\tau = \omega t - kz$ is preserved. As the electric field propagates in z-direction, the components $E_x(z,t), E_y(z,t)$ generate a resultant vector describing a locus of points in space. The polarization ellipse is then, the curve generated by the set of points that describes the electric field. To find that curve, we have the next equations

$$E_x(z,t) = E_{0x}\cos(\tau + \delta_x) \tag{1.72a}$$

$$E_y(z,t) = E_{0y}\cos(\tau + \delta_y) \tag{1.72b}$$

that can be rewritten as

$$\frac{E_x}{E_{0x}} = \cos(\tau + \delta_x) \tag{1.73a}$$

$$\frac{E_y}{E_{0y}} = \cos(\tau + \delta_y) \tag{1.73b}$$

Using the trigonometric identity $\cos(A + B) = \cos A \cos B - \sin A \sin B$

$$\frac{E_x}{E_{0x}} = \cos\tau\cos\delta_x - \sin\tau\sin\delta_x \tag{1.74a}$$

$$\frac{E_y}{E_{0y}} = \cos\tau\cos\delta_y - \sin\tau\sin\delta_y \tag{1.74b}$$

Multiplying by $\sin\delta_y$ and $\sin\delta_x$, respectively, we have

$$\frac{E_x}{E_{0x}}\sin\delta_y = \cos\tau\cos\delta_x\sin\delta_y - \sin\tau\sin\delta_x\sin\delta_y \tag{1.75a}$$

$$\frac{E_y}{E_{0y}}\sin\delta_x = \cos\tau\cos\delta_y\sin\delta_x - \sin\tau\sin\delta_y\sin\delta_x \tag{1.75b}$$

Subtracting those equations

$$\frac{E_x}{E_{0x}}\sin\delta_y - \frac{E_y}{E_{0y}}\sin\delta_x = \cos\tau\cos\delta_x\sin\delta_y - \cancel{\sin\tau\sin\delta_x\sin\delta_y}$$
$$- \cos\tau\cos\delta_y\sin\delta_x + \cancel{\sin\tau\sin\delta_y\sin\delta_x} \tag{1.76}$$

$$\frac{E_x}{E_{0x}}\sin\delta_y - \frac{E_y}{E_{0y}}\sin\delta_x = \cos\tau\cos\delta_x\sin\delta_y - \cos\tau\cos\delta_y\sin\delta_x$$
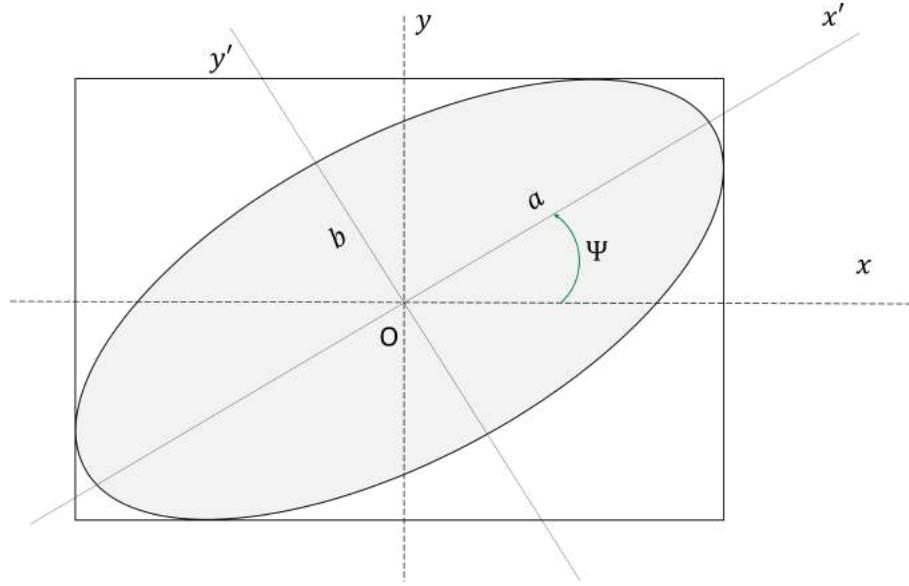
Figure 1.5: The polarization ellipse rotated.

Using the trigonometric identity $\sin(A - B) = \sin A \cos B - \cos A \sin B$, we have

$$\frac{E_x}{E_{0x}} \sin \delta_y - \frac{E_y}{E_{0y}} \sin \delta_x = \cos \tau \sin(\delta_y - \delta_x) \tag{1.77}$$

Going back to eqs. 1.74, we repeat the same procedure but this time multiplying by $\cos \delta_x$ and $\cos \delta_y$ to get

$$\frac{E_x}{E_{0x}} \cos \delta_y - \frac{E_y}{E_{0y}} \cos \delta_x = \sin \tau \sin(\delta_y - \delta_x) \tag{1.78}$$

Squaring eq. 1.77 and eq. 1.78 and adding them together, we obtain

$$\frac{E_x^2}{E_{0x}^2} + \frac{E_y^2}{E_{0y}^2} - 2 \frac{E_x}{E_{0x}} \frac{E_y}{E_{0y}} \cos \delta = \sin^2 \delta \tag{1.79}$$

where $\delta = \delta_y - \delta_x$. Finally, this expression is the ellipse equation. This ellipse is called **polarization ellipse** and it is rotated because it is not coincident with the coordinate axes, we know that due to the cross term $E_x E_y$.

Let x y y the initial unrotated axes and let x' and y' be the new set of rotated axes as in Figure 1.5. Futhermore, let $\Psi(0 \leq \Psi \leq \pi)$ be the angle between x and the direction x' of the major axis. The components E_x' y E_y' are [2]

$$\begin{pmatrix} E_x' \\ E_y' \end{pmatrix} = \begin{pmatrix} \cos \Psi & \sin \Psi \\ -\sin \Psi & \cos \Psi \end{pmatrix} \begin{pmatrix} E_x \\ E_y \end{pmatrix} \tag{1.80}$$

So we have

$$E'_x = E_x \cos \Psi + E_y \sin \Psi \tag{1.81a}$$

$$E'_y = -E_x \sin \Psi + E_y \cos \Psi \tag{1.81b}$$

Considering the standard form of the ellipse

$$\frac{E'^2_x}{a^2} + \frac{E'^2_y}{b^2} = 1 \tag{1.82}$$

with

$$E'_x = a \cos(\tau + \delta') \tag{1.83a}$$

$$E'_y = \pm b \sin(\tau + \delta') \tag{1.83b}$$

where a is the semimajor and b semiminor axes of the polarization ellipse and δ' an arbitrary phase. If we substitute the equations 1.74 and 1.83 into eq. 1.81 we have

$$
\begin{aligned}
a(\cos \tau \cos \delta' - \sin \tau \sin \delta') &= E_{0x}(\cos \tau \cos \delta_x - \sin \tau \sin \delta_x) \cos \Psi ... \\
&\quad ... + E_{0y}(\cos \tau \cos \delta_y - \sin \tau \sin \delta_y) \sin \Psi
\end{aligned}
\tag{1.84}
$$

and

$$
\begin{aligned}
\pm b(\sin \tau \sin \delta' + \cos \tau \sin \delta') &= -E_{0x}(\cos \tau \cos \delta_x - \sin \tau \sin \delta_x) \sin \Psi ... \\
&\quad ... + E_{0y}(\cos \tau \cos \delta_y - \sin \tau \sin \delta_y) \cos \Psi
\end{aligned}
\tag{1.85}
$$

Expanding the products and equating the coefficients we have that

$$a \cos \delta' = E_{0x} \cos \delta_x \cos \Psi + E_{0y} \cos \delta_y \sin \Psi \tag{1.86a}$$

$$a \sin \delta' = E_{0x} \sin \delta_x \cos \Psi + E_{0y} \sin \delta_y \sin \Psi \tag{1.86b}$$

$$\pm b \cos \delta' = E_{0x} \sin \delta_x \sin \Psi - E_{0y} \sin \delta_y \cos \Psi \tag{1.86c}$$

$$\pm b \sin \delta' = E_{0x} \cos \delta_x \sin \Psi - E_{0y} \cos \delta_y \cos \Psi \tag{1.86d}$$

Squaring the previous equations we obtain

$$a^2 = E^2_{0x} \cos^2 \Psi + E^2_{0y} \sin^2 \Psi + 2E_{0x}E_{0y} \cos \Psi \sin \Psi \cos \delta \tag{1.87a}$$

$$b^2 = E^2_{0x} \sin^2 \Psi + E^2_{0y} \cos^2 \Psi - 2E_{0x}E_{0y} \cos \Psi \sin \Psi \cos \delta \tag{1.87b}$$

Adding both equations, we have

$$a^2 + b^2 = E_{0x}^2 + E_{0y}^2 \tag{1.88}$$

Dividing the equation 1.86 by each other,

$$(E_{0x}^2 + E_{0y}^2) \sin 2\Psi = 2E_{0x}E_{0y} \cos \delta \cos 2\Psi \tag{1.89}$$

or

$$\tan 2\Psi = \frac{2E_{0x}E_{0y} \cos \delta}{E_{0x}^2 - E_{0y}^2} \tag{1.90}$$

In this way it has been possible to relate the angle of rotation Ψ with E_{0x}, E_{0y} and δ. If we introduce an auxiliary angle α defined as

$$\tan \alpha = \frac{E_{0y}}{E_{0x}} \tag{1.91}$$

the eq. 1.90 can be rewritten as

$$\tan 2\Psi = 2\frac{\tan \alpha}{1 - \tan^2 \alpha} \cos \delta \tag{1.92}$$

this leads to

$$\tan 2\Psi = \tan 2\alpha \cos \delta \tag{1.93}$$

Now, if we multiply the equations 1.86 between them, we have

$$\pm ab = E_{0x}E_{0y} \sin \delta \tag{1.94}$$

The ellipticity χ is another important parameter defined as

$$\tan \chi = \frac{\pm b}{a} \tag{1.95}$$

where $\chi(-\pi/4 \leq \chi \leq \pi/4)$. Using the auxiliary angle

$$\sin 2\chi = \frac{2E_{0x}E_{0y} \sin \delta}{E_{0x}^2 + E_{0y}^2} = \sin 2\alpha \sin \delta \tag{1.96}$$

1.4.3   Stokes polarization parameters

Unlike the Jones vectors, the Stokes parameters allow describing polarized, partially polarized and unpolarized light, so it can be said that they are complementary. The

Stokes parameters are a way to describe the polarization behavior in terms of observables because they do not involve the amplitude but the intensity which, if we remember from subsection 1.1.1 is the time average of the square of the amplitude. To derive the Stokes parameters it is required to make use of the wave theory [2]. Since the polarization ellipse is valid only at an instant of time, the eq. 1.79 can be written as

$$\frac{E_x^2(t)}{E_{0x}^2(t)} + \frac{E_y^2(t)}{E_{0y}^2(t)} - 2\frac{E_x(t)E_y(t)}{E_{0x}(t)E_{0y}(t)}\cos\delta(t) = \sin^2\delta(t) \tag{1.97}$$

where $\delta(t) = \delta_y(t) - \delta_x(t)$. If we considered monochromatic radiation, theoretically, the amplitudes and phases are constant all time [2], so the expression 1.97 is now

$$\frac{E_x^2(t)}{E_{0x}^2} + \frac{E_y^2(t)}{E_{0y}^2} - 2\frac{E_x(t)E_y(t)}{E_{0x}E_{0y}}\cos\delta = \sin^2\delta \tag{1.98}$$

in this way, E_{0x}, E_{0y} remain constant while E_x, E_y change in time. In order to work in terms of observable of the optical field, the observation is averaged over time, so that

$$\frac{\langle E_x^2(t)\rangle}{E_{0x}^2} + \frac{\langle E_y^2(t)\rangle}{E_{0y}^2} - 2\frac{\langle E_x(t)E_y(t)\rangle}{E_{0x}E_{0y}}\cos\delta = \sin^2\delta \tag{1.99}$$

where

$$\langle E_i(t)E_j(t)\rangle = \lim_{t\to\infty}\frac{1}{T}\int_0^T E_i(t)E_j(t)dt \quad i,j = x,y \tag{1.100}$$

Multiplying this equation by $4E_{0x}^2 E_{0y}^2$ we see that

$$4E_{0y}^2\langle E_x^2(t)\rangle + 4E_{0x}^2\langle E_y^2(t)\rangle - 8E_{0x}E_{0y}\langle E_x(t)E_y(t)\rangle\cos\delta = (2E_{0x}E_{0y}\sin\delta)^2 \tag{1.101}$$

The average values are

$$\langle E_x^2(t)\rangle = \frac{1}{2}E_{0x}^2 \tag{1.102a}$$

$$\langle E_y^2(t)\rangle = \frac{1}{2}E_{0y}^2 \tag{1.102b}$$

$$\langle E_x(t)E_y(t)\rangle = \frac{1}{2}E_{0x}E_{0y}\cos\delta \tag{1.102c}$$

Substituting equations 1.102 into 1.101 yields

$$2E_{0x}^2 E_{0y}^2 + 2E_{0x}^2 E_{0y} - (2E_{0x}E_{0y}\cos\delta)^2 = (2E_{0x}E_{0y}\sin\delta)^2 \tag{1.103}$$

Completing the square to have the expression in terms of intensity,

$$(E_{0x}^2 + E_{0y}^2)^2 - (E_{0x}^2 - E_{0y}^2)^2 - (2E_{0x}E_{0y}\cos\delta)^2 = (2E_{0x}E_{0y}\sin\delta)^2 \qquad (1.104)$$

Now, the quantities inside the parentheses will be the Stokes parameters, so that

$$S_0 = E_{0x}^2 + E_{0y}^2 \qquad (1.105a)$$

$$S_1 = E_{0x}^2 - E_{0y}^2 \qquad (1.105b)$$

$$S_2 = 2E_{0x}E_{0y}\cos\delta \qquad (1.105c)$$

$$S_3 = 2E_{0x}E_{0y}\sin\delta \qquad (1.105d)$$

The expression 1.104 can be rewritten as

$$S_0^2 = S_1^2 + S_2^2 + S_3^2 \qquad (1.106)$$

This is how the Stokes parameters are obtained, where each of them represents real observable quantities of the optical field. The total intensity is found in the parameter S_0. The parameter S_1 describes the amount of linear polarization, either vertical or horizontal; S_2 contains information about linear polarization at $+45°$ or $-45°$. Finally the parameter S_3 tells us how much light is circularly polarized to the right or left. The Stokes parameters satisfy the relation

$$S_0^2 \geq S_1^2 + S_2^2 + S_3^2 \qquad (1.107)$$

If the light is completely polarized, then it is an equality, while for cases of partially polarized or unpolarized light it holds as an inequality. Another advantage of using of the Stokes parameters is to describe the degree of polarization P for any state of polarization

$$P = \frac{I_{pol}}{I_{tot}} = \frac{\sqrt{S_1^2 + S_2^2 + S_3^2}}{S_0} \qquad (1.108)$$

where I_{pol} is the intensity of the sum of the components of polarization and I_{tot} is the intensity of the beam, in addition $0 \leq P \leq 1$. The value of $P = 1$ is for the light completely polarized, $P = 0$ for light unpolarized and $0 < P < 1$ for light partially

polarized. The Stokes parameters can be arranged in a column vector written as

$$\mathbf{S} = \begin{pmatrix} S_0 \\ S_1 \\ S_2 \\ S_3 \end{pmatrix} = \begin{pmatrix} E_{0x}^2 + E_{0y}^2 \\ E_{0x}^2 - E_{0y}^2 \\ 2E_{0x}E_{0y}\cos\delta \\ 2E_{0x}E_{0y}\sin\delta \end{pmatrix} \tag{1.109}$$

This four-element column matrix is known as the Stokes vector, and although it is not a vector mathematically, this representation is useful. For example, the Stokes vector for unpolarized light is

$$\mathbf{S}^{un} = \begin{pmatrix} S_0 - \sqrt{S_1^2 + S_2^2 + S_3^2} \\ 0 \\ 0 \\ 0 \end{pmatrix}. \tag{1.110}$$

and for polarized light it is

$$\mathbf{S}^{p} = \begin{pmatrix} S_0 - \sqrt{S_1^2 + S_2^2 + S_3^2} \\ S_1 \\ S_2 \\ S_3 \end{pmatrix} \tag{1.111}$$

To represent partially polarized light, a superposition of completely polarized and unpolarized light is then considered, so that the associated Stokes vector is

$$\mathbf{S} = \begin{pmatrix} S_0 \\ S_1 \\ S_2 \\ S_3 \end{pmatrix} = (1-P)S_0 \begin{pmatrix} 1 \\ 0 \\ 0 \\ 0 \end{pmatrix} + PS_0 \begin{pmatrix} 1 \\ S_1/PS_0 \\ S_2/PS_0 \\ S_3/PS_0 \end{pmatrix} \tag{1.112}$$

where $0 \leq P \leq 1$. Another representation of partially polarized light consists of decomposing the beam into two fully polarized beams with orthogonal polarizations, that is

$$\begin{pmatrix} S_0 \\ S_1 \\ S_2 \\ S_3 \end{pmatrix} = \frac{1+P}{2P} \begin{pmatrix} PS_0 \\ S_1 \\ S_2 \\ S_3 \end{pmatrix} + \frac{1-P}{2P} \begin{pmatrix} PS_0 \\ -S_1 \\ -S_2 \\ -S_3 \end{pmatrix} \tag{1.113}$$

where $0 < P \leq 1$ y $PS_0 = \sqrt{S_1^2 + S_2^2 + S_3^2}$. The intensity of these two beams would be given by

$$S_0^1 = \frac{1}{2}S_0 + \frac{1}{2}\sqrt{S_1^2 + S_2^2 + S_3^2} \tag{1.114a}$$

$$S_0^2 = \frac{1}{2}S_0 - \frac{1}{2}\sqrt{S_1^2 + S_2^2 + S_3^2} \tag{1.114b}$$

$$\tag{1.114c}$$

Note that the intensities would be equal only when unpolarized light is considered, that is $S_1 = S_2 = S_3 = 0$

Stokes parameters and their relationship with the polarization ellipse

In this work it is of interest to find the relationship between the ellipse parameters and the Stokes parameters. The Stokes parameters describe a polarization state by relating the amplitudes and relative phases of the x and y electric field components according to eq. 1.105. To more conveniently describe the polarization state of a vector beam, the Stokes parameter equations can be used as Cartesian coordinates of a point on the Poincaré sphere.

$$S_0 = \sqrt{S_1^2 + S_2^2 + S_3^2} \tag{1.115a}$$

$$S_1 = S_0 \cos 2\theta \cos 2\delta \tag{1.115b}$$

$$S_2 = S_0 \cos 2\theta \sin 2\delta \tag{1.115c}$$

$$S_3 = S_0 \sin 2\theta \tag{1.115d}$$

Here $2\delta \in [0, 2\pi]$ is the azimuthal spherical coordinate, and $2\theta \in [0, \pi]$ is the radial spherical coordinate; these have a parallelism with the orientation and ellipticity angle of polarization which also happen to be twice the angles. The relationship between the Poincaré sphere coordinates and the polarization ellipse properties is shown in Figure 1.6. The linear polarization states lie on the equator of the sphere while the right and left circular polarization states on the north and south poles, respectively, and elliptical states are located in between the equator and the poles surface.

Poincaré sphere

Polarization ellipse

$$\vec{S} = (S_1, S_2, S_3) = (\cos 2\theta \cos 2\delta \,, \cos 2\theta \sin 2\delta \,, \sin 2\delta)$$
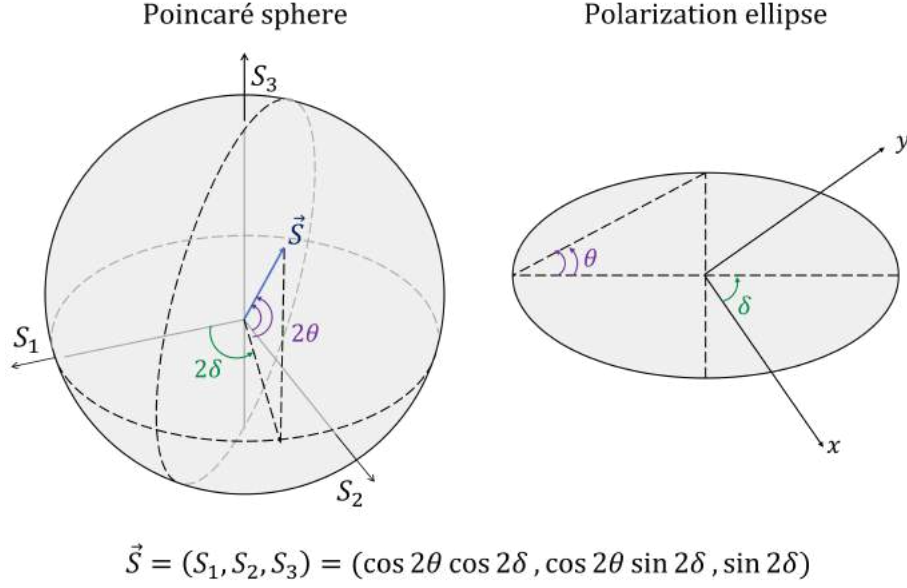
Figure 1.6: Relationship between the Poincaré sphere and the polarization ellipse. Diagram showing the relationship between the Cartesian coordinates of the Poincaré sphere and the ellipticity and orientation angles of the polarization ellipse.

Rearranging the Eqs. 1.115 b) and c) as

$$\frac{S_1}{S_0 \cos 2\theta \cos 2\delta} = \frac{S_2}{S_0 \cos 2\theta \sin 2\delta}$$
$$\delta = \frac{1}{2} \arctan\left(\frac{S_2}{S_1}\right)$$

(1.116)

Now, taking the sum in the quadrature of Eqs.1.115 b) and c) and equating to Eq. d) we obtain

$$\sqrt{S_1^2 + S_2^2} = \sqrt{S_0 \cos^2 2\theta(\cos^2 \delta + \sin^2 2\delta)}$$
$$\theta = \frac{1}{2} \arctan \frac{S_3}{\sqrt{S_1^2 + S_2^2}}$$

(1.117)

If we consider that $S_3 = I_R - I_L$ where I_R and I_L are the intensity distribution in right and left polarization state, we can see the handedness H_{CP} of any dominant circular polarization.

$$H_{CP} = \begin{cases} R & \text{for } S_3 > 0 \\ L & \text{for } S_3 < 0 \end{cases}$$

(1.118)

Using $\theta(x, y)$ as orientation, $\delta(x, y)$ as ellipticity and, $H_{CP}(x, y)$ as handedness we can determined the polarization ellipse at every point in a given field using the Stokes parameters [31].

Stokes polarimetry

The science that is responsible for measuring polarization is known as polarimetry. Various techniques exist to measure Stokes parameters. However, one of the most efficient is to measure four intensities. This method consists of a **Polarization State Analyzer (PSA)** composed of a phase retarder and a polarizer as well as a Charge-Coupled Device (CCD) camera. The intensity images obtained contain the necessary information to make the reconstruction of all the Stokes parameters and the state of polarization of the optical field. For a minimum of four intensity measurements, the associated Stokes parameters can be determined as

$$S_0 = I_R + I_L \tag{1.119a}$$

$$S_1 = 2I_H - S_0 \tag{1.119b}$$

$$S_2 = 2I_D - S_0 \tag{1.119c}$$

$$S_3 = I_R - I_L \tag{1.119d}$$

where I_H, I_D, I_L y I_R represent two-dimensional intensity profiles of the horizontal, diagonal, right circular, and left circular polarization components, respectively. In order to carry out the polarimetry using only these four intensity images, it is necessary to carry out projections in each of the polarization states. This is achieved by using a phase retarder: **Half-Wave plate retarder (HWP)** for linear, horizontal and diagonal measurements; **Quarter-Wave plate retarder (QWP)** for circular polarization, while the **Linear polarizer (LP)** is fixed in front of the CCD camera. The transmission axis of the retarder plate must be accommodated accordingly, for example, to obtain the horizontal polarization intensity image, the HWP is required to be at 0° while the diagonal measurement requires rotate to 22.5°. In the case of circular intensities, the QWP is required to be at ±45°, as appropriate to the left and right. Once these four images are obtained, using code, it is possible to reconstruct the Stokes parameters, the intensity profile for each of them, as well as the polarization distribution along the intensity profile of the beam.

1.5   Coherence

The optical property of coherence is a way of measuring the degree of correlation between the complex amplitudes that exist between the vibrations of the electromagnetic field in different places and times. A source is coherent if this degree of

correlation is fixed or constant. There is **temporal coherence** which measures how monochromatic the light is and **spatial coherence** which measures how stationary the phase is maintained along the optical wavefront. A monochromatic continuous wave source is coherent in time because it is composed of only one frequency, and it is coherent spatially because, all over the wavefront, the fluctuations between the relative phases of the field are zero. A laser can be considered as a highly coherent source because the spectral line width is narrow that is, they are quasimonochromatic and in their gain medium, the light produced maintains a correlated phase so it is coherent in space and time.

To study coherence, the Young's experiment shown in Figure 1.3 is relevant where a primary monochromatic source S illuminates two pinholes in a opaque screen that turn into two secondary point sources S_1 and S_2. Interference fringes can be observed on a distant screen Σ_0. At this point we already know that if S is an idealized source, the wavefronts from S_1 and S_2 are going to maintain a constant relative phase so they will be correlated and it is said that they are coherent. The interference pattern of stable fringes observed will be well-defined. On the other hand, if we use two different sources to illuminate the pinholes, no correlation exist between the wavefronts generated and then, no fringes will be observed even when the sources have very narrow bandwidths, so it is said that S_1 and S_2 are incoherent. For this reason, a way of knowing the coherence degree of a light source is through the sharpness or visibility of the interference fringes produced by the superposition of the vibrations emitted from two secondary point sources on the wavefront. The fringes are expected to be very sharp for a spatially coherent source because the correlation between the oscillating field amplitudes is high. As coherence is lost, these fringes will soften and little by little they will disappear until the correlation is null, it is there where the source is said to be incoherent. It is important to note that a real source is not completely coherent or incoherent, which is why the term partially coherent appears [28, 1, 29].

1.5.1   Extended source

Let's consider the double slit Young's experiment set up shown in Figure 1.7. An extended quasi-monochromatic light source S of diameter L and wavelength λ is located at a distance d from a opaque screen and illuminates two tiny apertures S_1 and S_2 separated by a distance a, and symmetrically located with respect to the optical axis. An observation plane perpendicular to the optical axis and parallel to the opaque screen with the apertures is placed where the interference fringes can be

observed [5]. When the light source is a monochromatic point source, the two holes become two coherent sources of light and interference fringes centered about the z-axis can be observed on the screen where the separation between them is proportional both to wavelength and screen distance and inversely proportional to the hole spacing [29].
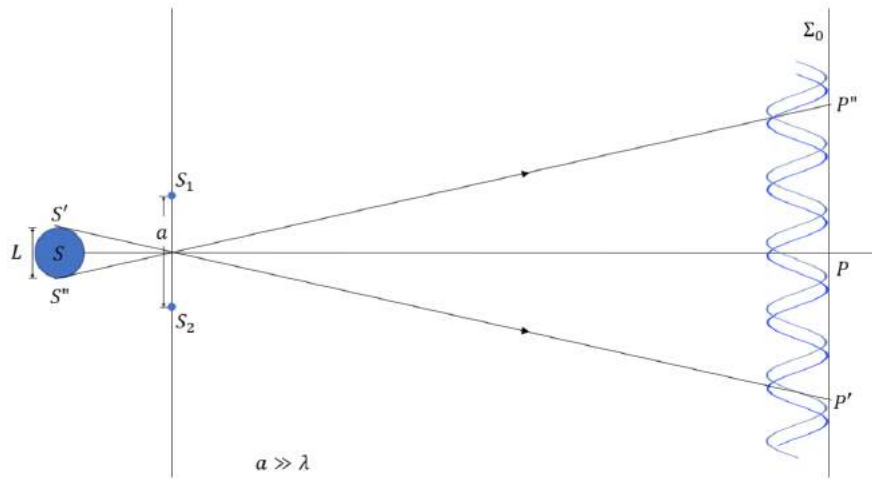
Figure 1.7: Interference experiment with an extended source.

If we take a secondary point source that is slightly shifted from the optical axis in the transverse plane like S' or $S"$ in Figure 1.7, the effect on the interference fringes will be a shift of the on-axis maximum. Therefore, an extended source is made up of a large number of point sources which are mutually incoherent due to the random phase fluctuation from each point source and this means that the intensity at any point in the wave-field is then the sum of the intensities from the individual point sources [5, 32]. The pattern observed of interference fringes will become more diffused as the transverse extent of the source increases, the spatial coherence of the source can be approximate by the condition $aL/d \leq \lambda/2$ however a more precise characterization require the study correlations between light coming from apertures S_1 and S_2.

1.6 Light modulators

In recent years, various technologies have been used to structure light. However, those that allow, through computer-controlled devices, to modify light at will in almost any way possible, have been of particular interest. Examples of these devices are Digital Micro-Mirror Device (DMD) and Spatial Light Modulators (SLM).

1.6.1 Digital Micro-Mirror Device

A Digital Micro-Mirror Device (DMD) is a device composed of a two-dimensional array of small mirrors that can be treated as pixels. Each mirror can be controlled individually and binary, that is, the mirror can only take one of two positions. These positions depend on the angle at which a mirror can be moved, and it varies depending on the model, but is generally between ± 12 and ± 17 degrees, with + being the on position and - being the off position [33, 34]. The Figure 1.8 is a DMD without the optical body and the black rectangles in the matrix represent the off pixels.
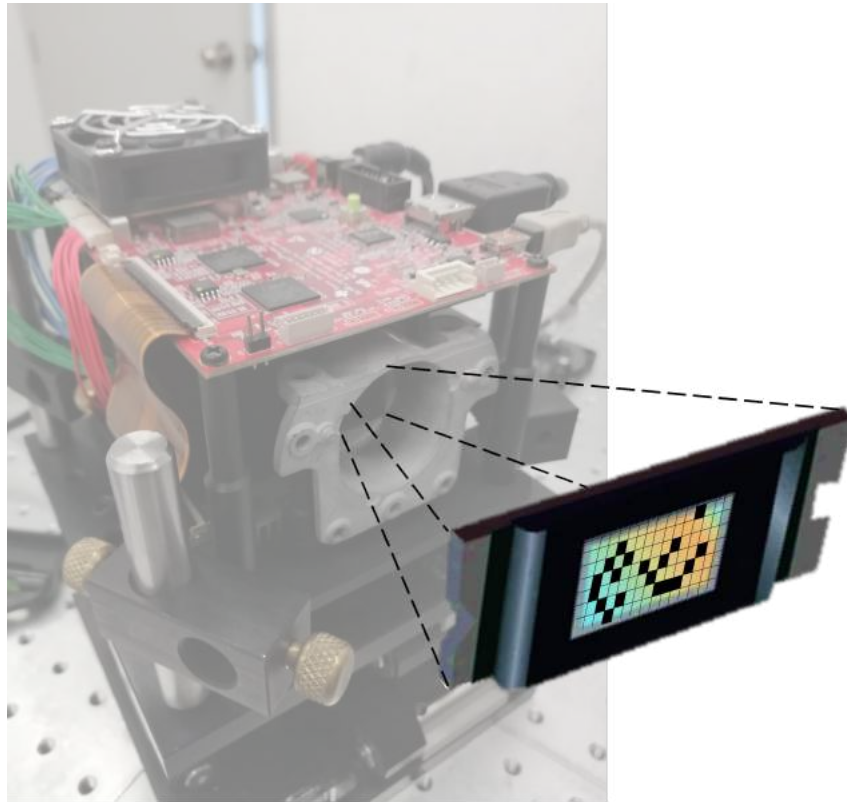
Figure 1.8: A Digital Micro-Mirror Device (DMD) without the optical body. The black rectangles in the matrix represent the off pixels.

As they are mirrors, a DMD is insensitive to incident wavelength and polarization and can only encode amplitude information and not phase information. It is known that modulating light requires confining both amplitude and phase in a computer generated hologram. Fortunately there are various holographic methods that use only amplitude modulation to structure light. In this work the method described by Arrizón "Complex amplitude modulation" and by Lee holograms are used. The rate of change at which a DMD connected to a computer is capable of displaying patterns is

60Hz but this can be improved by understanding how Digital Light Processing (DLP) projector works and how it creates a color image [35, 34]. Some considerations when working with DMDs is that the position in which it is placed will affect efficiency and fidelity, that is, the amount of light that first order diffraction receives and how identical the reflected modes are with the encoded modes. The most optimal way is to orient the DMD so that having all the mirrors turned off they are normal to the incident beam. However, it is important to note that efficiency is one of the main disadvantages of these devices because it only reaches close to 9% [35, 34]. Another consideration is that DMDs are not completely flat so they can introduce unwanted phases due to aberrations. One way to get rid of them is to encode a small beam, although this reduces efficiency and limits fidelity because fewer pixels are available. A better way to do it, although not easy, would be to counteract the added phases using the corresponding Zernike polynomial [34].

1.6.2   Spatial Light Modulator

Spatial Light Modulators SLMs can modulate light properties such as amplitude, polarization, and phase. Its operating principle consists of a two-dimensional array of pixels filled with liquid crystal. Each pixel can be controlled independently using voltage. The device is calibrated so that, at a certain voltage, the molecules rotate a predetermined angle, resulting in a kind of birefringent material for a specific orientation of input polarized light. Unlike DMDs, SLMs are polarization sensitive and can only modulate a single polarization of light, generally horizontal [36, 34]. A SLM is shown in Figure 1.9

Figure 1.9: A Spatial Light Modulator. The tiny screen is the array of pixels filled with liquid crystal.

The voltage, as well as the phase shift, can be controlled using a grayscale image that takes 256 colors where 0 is black and 2π is white keeping the gray diversity intermediate on a linear scale [36, 37]. One of the problems we have to face when we are working with SLMs is that a considerable part of the light is not modulated because it falls on the edges between the pixels so that this unmodulated light mixes with the modulated light. This problem can be solved by adding a blazed grid to spatially separate the modulated from the non-modulated light. This also causes the orders to propagate at different angles, which is why in the experimental arrangements we rely on spatial filters to isolate the desired one . SLMs usually present disadvantages in optical communication systems because they depend on the state of polarization, wavelength, low frame rate and high scattering [36, 37, 38].

Chapter 2

Vector beams

A **Vector Beam (VB)** is a spatial mode which is a spatial pattern of light that lies in the transversal plane tot the direction of propagation of the light beam [39] and it is a solution to the wave equation. A scalar beam is characterized by the fact that its polarization states are homogeneous, that is, they are the same at all point along the transverse plane of the light beam. On the other side, a VB have polarization states that are not spatially homogeneous.

Previously, it used to be believed that it was important that the VBs were solutions to the Helmholtz equation because, since this is a partial differential equation of time and space, this implies that the spatial pattern of the spatial mode is a solution to the wave equation and, as space and time change, that is, as the beam propagates, the spatial pattern does not change [39]. However, in recent years, beams whose modes change in space and even destroy and self-heal have been generated [40], as well as beams whose modes are not a solution to the Helmholtz equation, such as helico-conical beams [41].

The VBs that are discussed in this work are solutions to the Helmholtz vector wave equation in different coordinate systems. However, commonly they are generated as coaxial superposition of orthogonal scalar fields with scalar polarization as [42]

$$U(\mathbf{r}) = \exp(i\delta_1)\hat{\mathbf{e}}_{\mathbf{R}} + \exp(i\delta_2)\hat{\mathbf{e}}_{\mathbf{L}} \tag{2.1}$$

where the unit vectors $\hat{\mathbf{e}}_{\mathbf{R}}$ y $\hat{\mathbf{e}}_{\mathbf{L}}$ represent the right and left circular polarization with their respective amplitudes $u_R(\mathbf{r})$ and $u_L(\mathbf{r})$. Other way to represent a vector beam is

$$U(\mathbf{r}) = u_R(\mathbf{r})\cos\theta\hat{\mathbf{e}}_{\mathbf{R}} + u_L\sin\theta\exp(i\delta)\hat{\mathbf{e}}_{\mathbf{L}} \tag{2.2}$$

Here $\cos\theta$ y $\sin\theta$ are weighting factors while $\exp(i\delta)$ is the intermodal phase.

2.1   Weighting factors

In the equation 2.2, $\cos\theta$ y $\sin\theta$ are **weighting factors** or amplitude. By modifying the values of the angle θ, the orthogonal components acquire different values so different vector beams are obtained. By the variation of θ one of the polarization components can even be eliminated and then a scalar beam will be produced. The values that θ can take range from 0 to $\pi/2$.
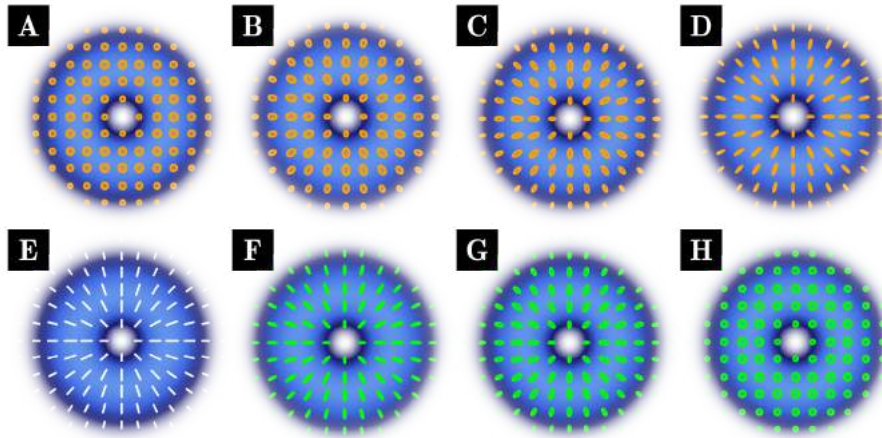
Figure 2.1: Beams with different values of θ: A) 0, B) $\pi/16$, C) $\pi/8$, D) $3\pi/8$, E) $\pi/4$, F) $5\pi/16$, G) $3\pi/8$, H) $\pi/2$. Note that all of them are vector beams except A and H. The right circular polarization is represented with orange circles while the left one with green ones. The linear polarization is represented with white lines. Other intermediate polarization states are represented with orange and green ellipses

In Figure 2.1 we can see different beams for different values of θ and how they pass from an scalar beam who has a homogeneous distribution of right circular polarization when $\theta = 0$) which is represented with orange circles to scalar beam with left circular polarization which occurs when $\theta = \pi/2$ and we have green circles to represent them. In this transition, vector beams are present. We can notice a transition from circles to ellipses and a reorganization of each polarization ellipse into a radial orientation and, just in the middle of the way, when $\theta = \pi/4$, we have the radial mode where we have linear polarization represented with those white lines pointing to the center of the vector mode.

2.1.1 Intramodal and intermodal phase

The intramodal and intermodal phase of a beam are two different concepts that are often confused and interchanged with each other as if they were synonymous. However, they are two different ideas that start from the conception of intrasystems and intersystems in entanglement [43]. A **intrasystem entanglement** is when different degrees of freedom of a single system are entangled. A **intersystem entanglement** is entaglement between physically distinct systems. In this way, we can define that the **intramodal phase** is a phase between the two components of the helical mode, the even and the odd [44]. The **intermodal phase** is a difference or a delay between both polarization components of the spatial modes[42, 45]. The difference is inside the exponential term as δ in equation 2.2 and goes from 0 to π.
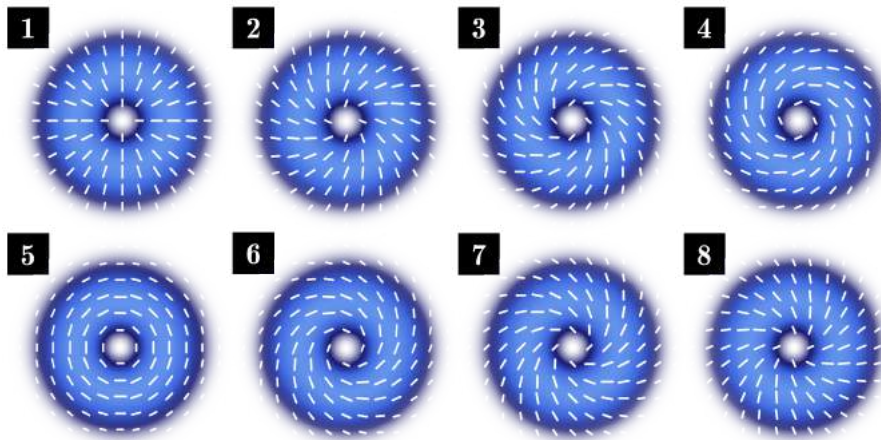
Figure 2.2: Vector beams with different values of δ. The intermodal phase can be geometrically interpreted as the rotation of each one of the polarization ellipses.

In Figure 2.2 we can see the transition of a radial mode in A) to an azimuthal polarization E) passing through spiral clockwise polarization and then, from F) to H), we have a spiral vector beams again but counter-clockwise this time.

2.2 High Order Poincaré sphere
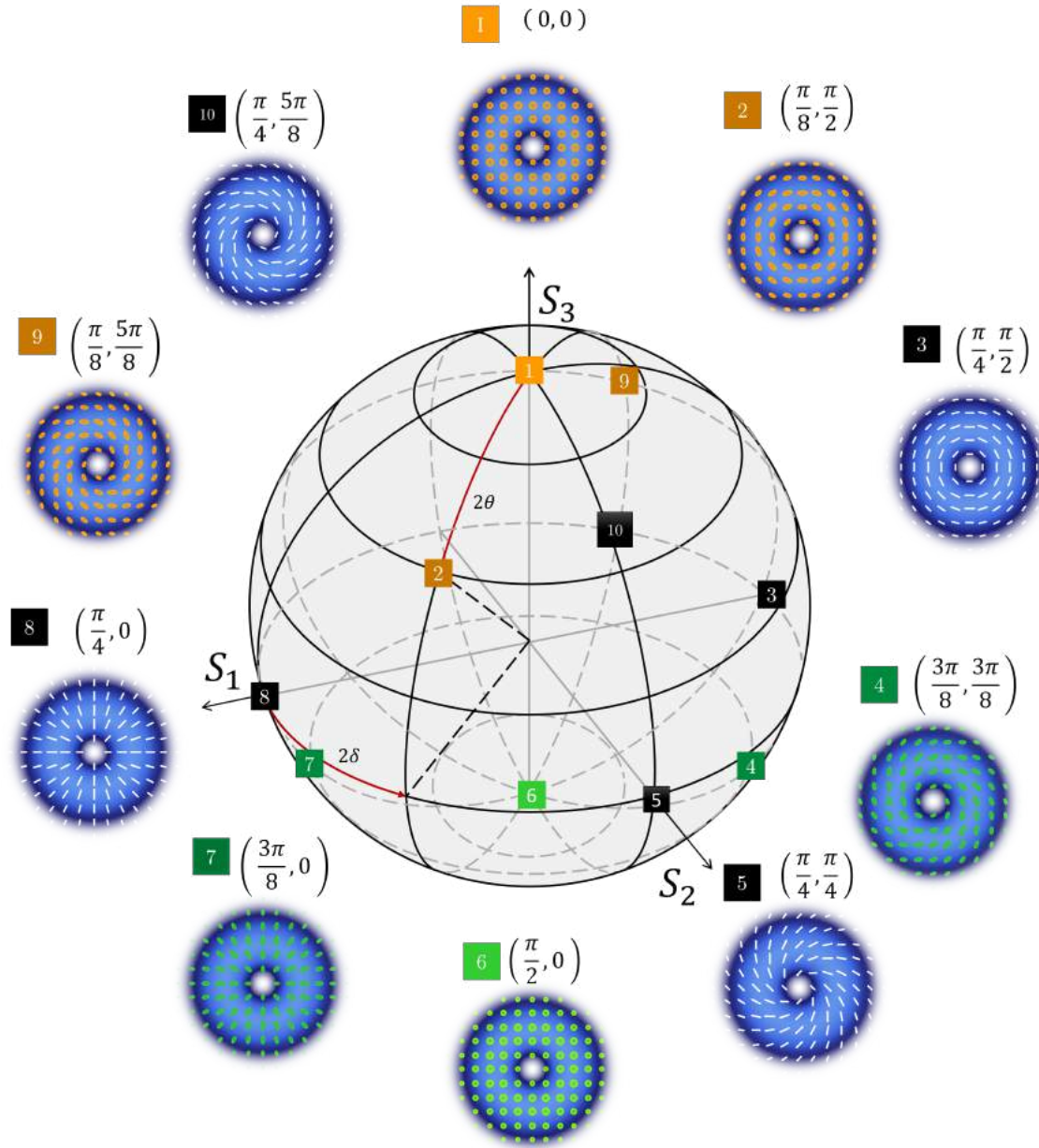
Figure 2.3: High Order Poincaré Sphere (HOPS) with some polarization states represented on it according to coordinates $(2\theta, 2\delta)$. Those states located in the same parallel or meridian are indicated with the same square color number.

As observed in the previous subsections, if the weight factors or the intermodal phase are modified, various types of polarization distributions are obtained. Then, if both angles are modified simultaneously, an infinite number of vector beams with very different polarization distributions can be obtained, and one way of visualizing them

is through the **High Order Poincaré Sphere (HOPS)**.

Resuming, by varying the value of the angle θ or by modulating the weight factors, the polarization can be transformed along the longitudes on the HOPS for the northern hemisphere to the southern hemispher, going from beams circularly polarized scalars, passing through elliptical states until reaching the equator where linearly polarized beams meet. On the other hand, if the intermodal phase is modified, each of the polarization ellipses distributed in the beam polarization profile rotates in such a way that it can be said that by changing the angle δ, an azimuthal displacement (or parallel to the equator of the sphere) is obtained.

Some polarization states are represented in Figure 2.3 and how they change as one moves in the HOPS. For example, it can be seen in the poles of the sphere the the states of polarization 1) scalar right circular and 6) scalar left circular polarization. In the equator, the HOPS contain the linear polarization states represented with black square numbers: 3) azimutal, 5) clockwise spiral, 8) radial and 10) counterclockwise spiral polarized states. At other points on the sphere we have states of intermediate polarization with elliptical polarization in different orientations: 2) azimuthal right elliptical , 4) clockwise spiral left elliptical 7) radial left elliptical, 9) counterclockwise spiral right elliptical.

2.3   Helical Vector Beams

2.3.1   Helical Laguerre-Gauss Vector Beam

A **Helical Laguerre-Gaussian Vector Beam (HLGVB)** is built of two scalar modes HLG, one of them is even and the other is odd as shown in subsection 1.2.1 and which are mathematically described in equation 1.26.

$$\mathbf{HLGVB}^{\pm}_{l_1,l_2;m_1,m_2}(\rho,\phi,z) = \cos\theta \mathrm{LG}^{+}_{l_1,m_1}\hat{e}_R + \sin\theta\exp(i\delta)\mathrm{LG}^{-}_{l_2,m_2}\hat{e}_L \qquad (2.3)$$

$$\cos\frac{\pi}{2}\,\mathrm{HLG}(2,1)^+\hat{e}_R \qquad \sin\frac{\pi}{2}\,\exp\left(\mathrm{i}\frac{\pi}{4}\right)\mathrm{HLG}(2,1)^-\hat{e}_L \qquad \mathrm{HLGVB}(2,1)$$

Figure 2.4: Example of a generation of an Helical Laguerre-Gaussian Vector Beam (HLGVB).

A graphic representation of the equation 2.3 is shown in Figure 2.4 where a symmetrical HLGVB is represented ($l_1 = l_2 = 2$) and ($m_1 = m_2 = 1$). The way to indicate the symmetry in the beam in this work will be using only a parenthesis with the two indices in order, in this case, HLGVB (2,1). The weighted factor, $\theta = \pi/2$ and the intermodal phase is $\delta = \pi/4$.
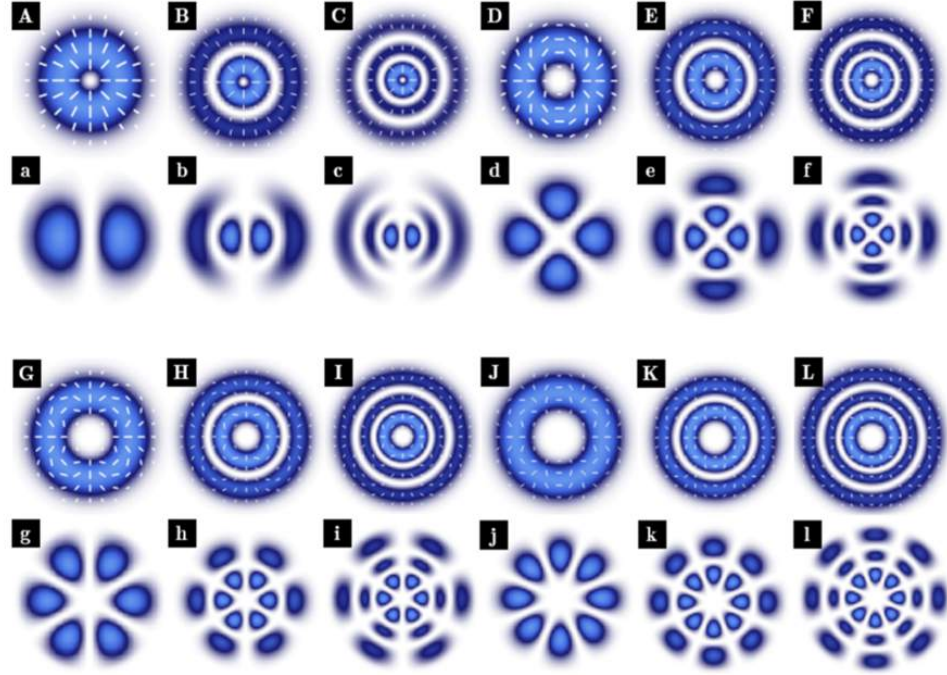
Figure 2.5: Helical Laguerre-Gaussian Vector Beams (HLGVBs). An intensity and polarization profile are represented with capital letters while with lowercase letters are used to name a projection of the intensity profile in the horizontal direction of the linear polarizer. In Figure, Aa. (1,0) Bb. (1,1), Cc. (1,2), Dd. (2,0), Ee. (2,1), Ff. (2,2) Gg. (3,0), Hh. (3,1), Ii. (3,2), Jj. (4,0), Kk. (4,1) and Ll. (4,2) where (l,m)

In Figure 2.5, different symmetrical HLGVBs are represented. The numbers in parenthesis, as it was previously discussed in 1.2.1, represent the number of petals $(2l)$ and the number of rings $(m+1)$.

2.3.2 Helical Ince-Gauss Vector modes

The **Helical Ince-Gaussian Vector Beam (HIGVB)** are built by a linear combination of the even and odd HIG beams

$$\mathbf{HIGVB}^{\pm}_{p,m,e}(\xi,\eta) = \cos\theta \mathrm{HIG}^{e}_{p,m,\epsilon}\hat{e}_R + \sin\theta \exp(i\delta)\mathrm{HIG}^{o}_{p,m,\epsilon}\hat{e}_L \qquad (2.4)$$

where $\theta\epsilon[0,\pi/2]$ is the associated angle to the weighted factors and $\delta\epsilon[0,\pi]$ is related to the intermodal phase.

$$\cos\frac{\pi}{4}\,\mathrm{HIG}(1,3)^{+}\hat{e}_{R} \qquad \sin\frac{\pi}{4}\,\mathrm{HIG}(1,3)^{-}\hat{e}_{L} \qquad \mathrm{HIGVB}(1,3)$$
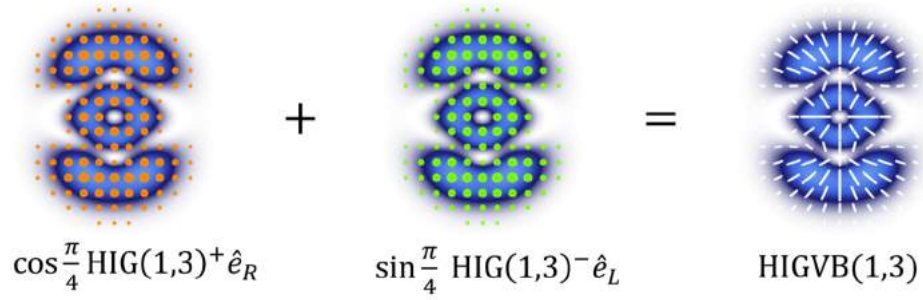
Figure 2.6: Example of a generation of an Helical Ince-Gaussian Vector Beams (HIGVBs).

A graphic representation of the equation 2.4 is shown in Figure 2.6 where an HIGVB is represented with $m = 1$, $p = 3$ and eccentricity of 0.4. The weighted factor, $\theta = \pi/4$ and the intermodal phase is $\delta = 0$ this is the reason of why the factor $\exp(i\delta)$ is equal to one and does not appear.
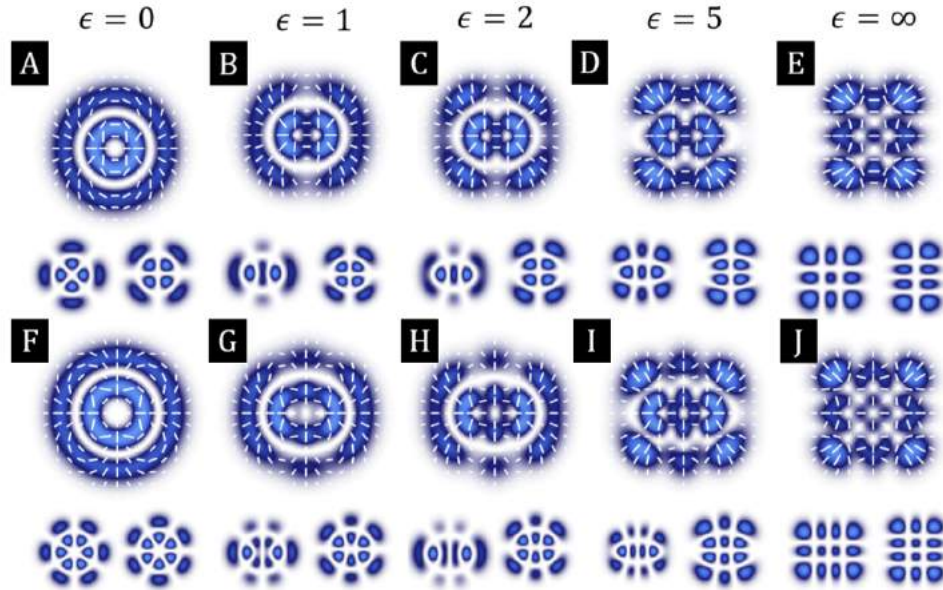
Figure 2.7: Helical Ince-Gaussian Vector Beams (HLGVBs) from A) to E) an even mode $\mathbf{HIGVB}(2,4)$ with different eccentricity and, from F) to J) an odd $\mathbf{HIGVB}(3,4)$. An intensity and polarization profile is shown. Under it, the horizontal and vertical projections of the intensity profile of the linear polarizer.

In Figure 2.7, two different symmetrical HIGVBs are represented. In the first row, a even HIGVB and in the second one, a odd mode. Both cases with different eccentricities. Under the distribution of polarization, there are the two projections in

the linear polarizer of the intensity profile, the horizontal and the vertical one. Notice how the sum of both generates the complete intensity mode.

2.3.3   Helical Mathieu Gauss Vector Beams

The **Helical Mathieu-Gaussian Vector Beam (HMGVB)** are generates as a non-separable superposition of the polarization and spatial degrees of freedom encoded in the HMG beams [27].

$$\textbf{HMGVB}_{m_1,m_2} = \cos\theta \text{HMG}^+_{m_1}\hat{e}_R + \sin\theta\exp(i\delta)\text{HMG}^-_{m_2}\hat{e}_L \tag{2.5}$$

where we omit the explicit depedence on $(\xi,\eta,z;q)$. The functions $\text{HMG}^\pm_{\text{m}}$ represent the HMG modes given by equations 1.38.
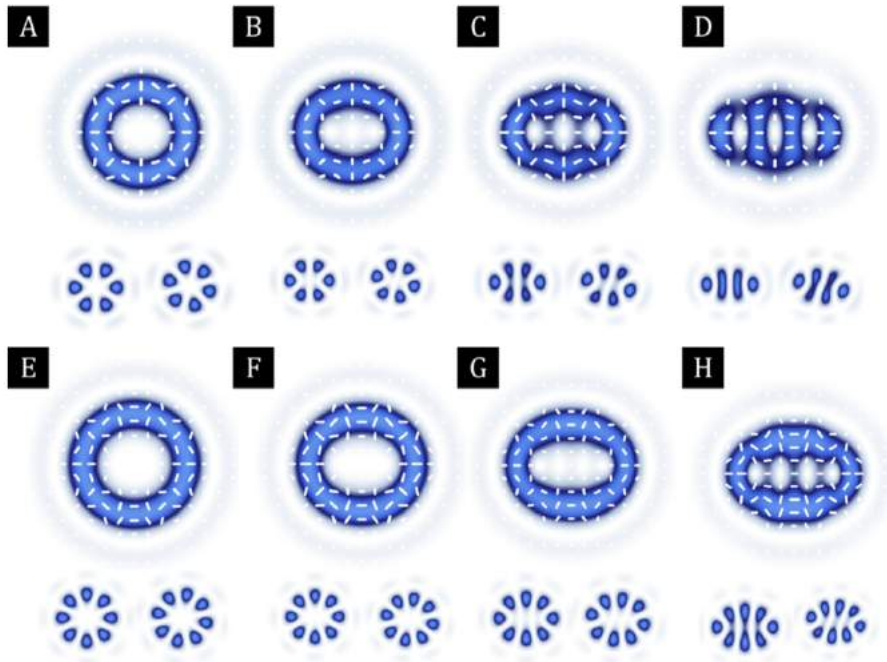
Figure 2.8: Helical Mathieu-Gaussian Vector Beams (HMGVBs) from A) to D) an odd mode **HMGVB**$(3,3)$ with different eccentricity and, from E) to H) an even **HMGVB**$(4,4)$. An intensity and polarization profile is shown. Under it, the horizontal and diagonal projections of the intensity profile of the linear polarizer.

In Figure 2.8, two different symmetrical **HMGVBs** are represented. In the first row, a odd **HMGVB** and in the second one, an even mode. Both cases with different eccentricities. Under the distribution of polarization, there are the two projections in

the linear polarizer of the intensity profile, the horizontal and the diagonal one.

2.4 Generation of vector beams

Once we understand the main parameters of vector beams, we can generate them experimentally. We used two experimental setup with a DMD (DLCR4710EVM-G2 with pixel size 5.4μm from Texas Instruments) one of them with a common-path interferometer, known to be highly stable [46] and the other using only a polarizing beam splitter to generate the vector beam [27, 47]. Next, each of the experimental setups will be described precisely and the vector beams generated with each of them will be shown.

2.4.1 Generation of vector beams through a common-path interferometer

The technique consists of a continuous wave laser beam ($\lambda = 633$nm) with horizontal polarization that is expanded and collimated by a Microscope Objective (MO) and lens L_1. The wavefront then passes through a Spatial Filter (SF) to approximate a flat wavefront and is sent through a HWP oriented at $22.5°$ to convert its horizontal polarization to diagonal polarization, $+45°$. The lens system made up of L_2 and L_3 form a telescope to image the flat wavefront onto the DMD. In the DMD screen are displayed two multiplexed binary holograms, which contain the amplitude and phase information of the constituting orthogonal modes. Each hologram has a unique linear phase grating to separate each orthogonal mode through different propagation directions so that when the flat wave front impinges the screen of the DMD, two orthogonal modes with diagonal polarization travel along different paths in the first diffraction order which is filtered from the higher diffraction orders by a SF. Both orthogonal modes fed a Sagnac interferometer made up by a Polarizer Beam Splitter (PBS) and two mirrors (M_1, M_2). The PBS divides both beams with diagonal polarization in the two components: horizontal and vertical which travels along different directions but in the same optical path. The mirrors are orientated to overlap the order that carry both orthogonal polarization components and the other two modes are filtered with a SF so, at the output of the Sagnac interferometer, we have a vector beam in the linear basis polarization. A QWP is used to change the polarisation from the linear basis to the circular polarisation basis. To do this, the QWP must be oriented with its fast axis at $+45°$. The lens L_3 and L_4 conform a 4f optical system between

the DMD and the charged couple device (CCD DCX Thorlabs, 4.65μm pixel size) which is used to observe and characterize the vector modes. A LP, a QWP and a HWP are used to the characterization of the beam. The method used to do this is to reconstruct the Stokes parameters with four intensity measurements associated to left and right circular polarization, horizontal and diagonal polarization. A LP orientated at 0° before the CCD camera is necessary and, to take the intensity associated with horizontal and diagonal polarization is used a HWP with its axis orientated at 0° and 22.5° respectively. The circular polarization left and right are measured with the aim of a QWP with its fast axis at +45° and −45° to obtain right and left polarization, respectively.
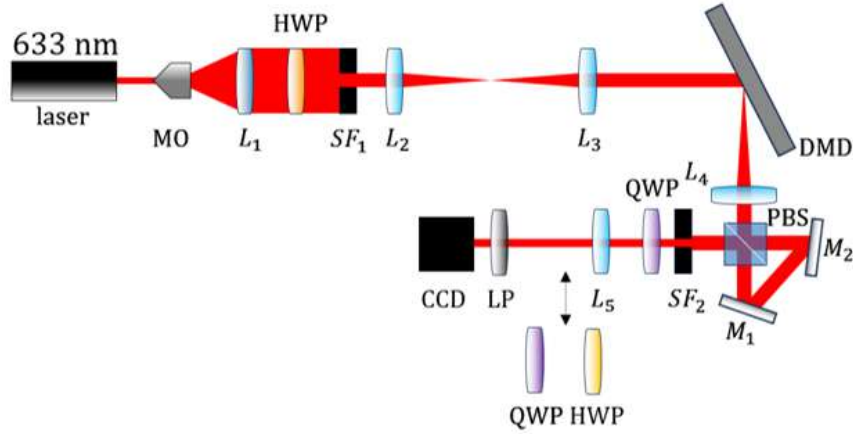
Figure 2.9: Schematic representation of the experimental setup with common-path interferometer.

The vector beams obtained using this technique are shown in Figure 2.10 where a comparison between the results obtained experimentally and the numerical simulations of beams from various families are presented. In Figure 2.10 we observe the example of a) LGVB$(1,0)$ with $\theta = \pi/4$, $\delta = 0$ and $W_0 = 0.5$, b) LGVB$(1,0)$ with $\theta = \pi/4$, $\delta = \pi/2$ and $W_0 = 0.5$, c) HIGVB$(3,5)$ with $\theta = \pi/4$,$\delta = \pi$, $W_0 = 0.5$ and $e = 2$ d) HMGVB$(4,4)$ with $\theta = \pi/4$,$\delta = 0$, $W_0 = 1.0$, $e = 0.5$,$a = 1$,$k_t = 6$, $z = 0$. The intensity distributions in the theoretical right (R) and left (L) circular polarization and horizontal (H) and, diagonal (D) polarization projections are displayed at the left side of the experimentally extracted intensity profiles for the vector beam of interest measured by the technique previously described in Subsection 1.4.3.
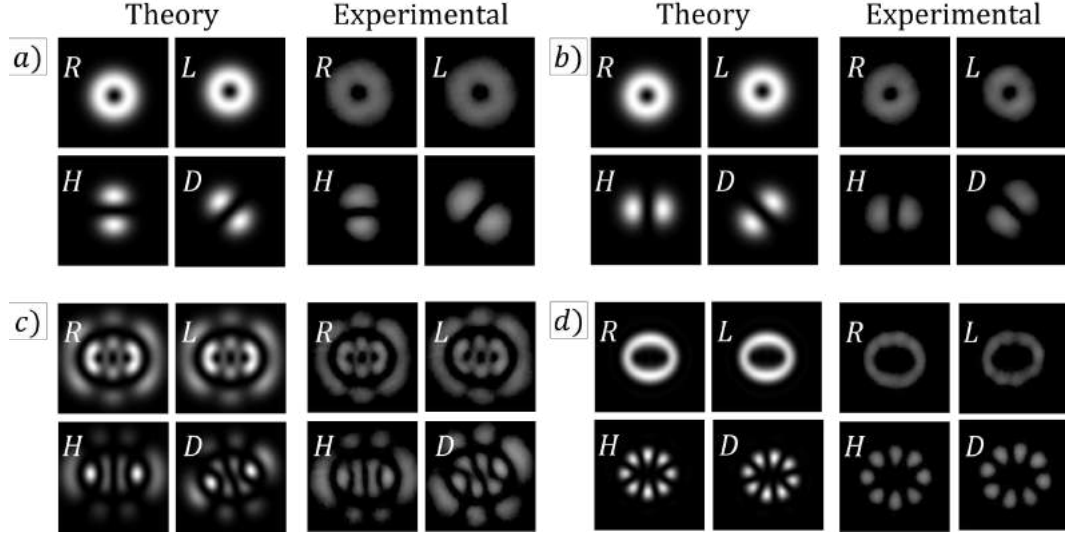
Figure 2.10: Vector Beam intensity distributions in its polarization projections. A theoretical intensity distributions in its polarization projections of a) LGVB$(1,0)$ with $\theta = \pi/4$, $\delta = 0$ and $W_0 = 0.5$, b) LGVB$(1,0)$ with $\theta = \pi/4$, $\delta = \pi/2$ and $W_0 = 0.5$, c) HIGVB$(3,5)$ with $\theta = \pi/4$, $\delta = \pi$, $W_0 = 0.5$ and $e = 2$ d) HMGVB$(4,4)$ with $\theta = \pi/4$, $\delta = 0$, $W_0 = 1.0$, $e = 0.5$, $a = 1$, $k_t = 6$, $z = 0$ with its experimental measurements. R and L represent the intensity distribution in its right and left circular polarization projection, respectively. H and D are the intensity distributions in its horizontal and diagonal projection. ($\lambda = 633$ nm)

The Stokes parameters were calculated using the intensity profiles in Figure 2.10 according to the Eqs. 1.119. It is evident that there is very good agreement between the experimentally extracted Stokes parameters and those predicted theoretically as we can see in Figure 2.11. The same occurs to the state of Polarization reconstruction (PR) with its simulated prediction.

Figure 2.11: Stokes parameters of Vector Beams. A contrast between a theoretical a) LGVB$(1,0)$ with $\theta = \pi/4$, $\delta = 0$ and $W_0 = 0.5$, b) LGVB$(1,0)$ with $\theta = \pi/4$, $\delta = \pi/2$ and $W_0 = 0.5$, c) HIGVB$(3,5)$ with $\theta = \pi/4$, $\delta = \pi$, $W_0 = 0.5$ and $e = 2$ d) HMGVB$(4,4)$ with $\theta = \pi/4$, $\delta = 0$, $W_0 = 1.0$, $e = 0.5$, $a = 1$, $k_t = 6$, $z = 0$ and its experimental Stokes polarization reconstruction. I_0 represent the intensity of the vector mode, S_0, S_1, S_2 and S_3 represent the intensity for each Stokes parameter and PR is the polarization reconstruction of the vector beam. ($\lambda = 633nm$)

2.4.2 Generation of vector beams through a polarizing beam splitter

The experimental setup consists of a continuous wave laser beam ($\lambda = 633nm$) with diagonal polarization that is expanded and collimated by a MO and lens L_1. The beam passes through a SF to approximate a flat wavefront. The lenses L_2 and L_3 conform a telescope that will make image of the flat wavefront into the DMD screen but before that, the beam is separated into its vertical and horizontal polarization components by a PBS. Both polarization components are directed toward the DMD where they spatially overlap but impinge under slightly different angles. The DMD shape phase and amplitude of both polarization by a multiplexed hologram. The first diffraction order, which contain both polarization states, propagates along a common axis. The SF removes the higher orders of diffraction. The lenses L_4 and L_5 formed a 4f optical system to relay the plane of the DMD into the detector's plane (CCD DCX Thorlabs, 4.65μm pixel size) which is also the observation plane. A QWP oriented at $+45°$ is placed afterwards to convert the linear polarization basis into circular one. Here, the optical train of generation of a vector beam is over. The analyzer part is formed by a LP, HWP and a QWP that is going to used to obtain the intensity profile of each one of the four measurements needed to characterize the vector beam. The LP is fixed in front of the CCD camera while the transmission axis of the retarder plate must be accommodated accordingly, for example, to obtain the horizontal polarization intensity image, the HWP is required to be at $0°$ while the diagonal measurement requires rotate to $22.5°$. In the case of circular intensities, the QWP is required to be at $\pm45°$, as appropriate to the left and right.
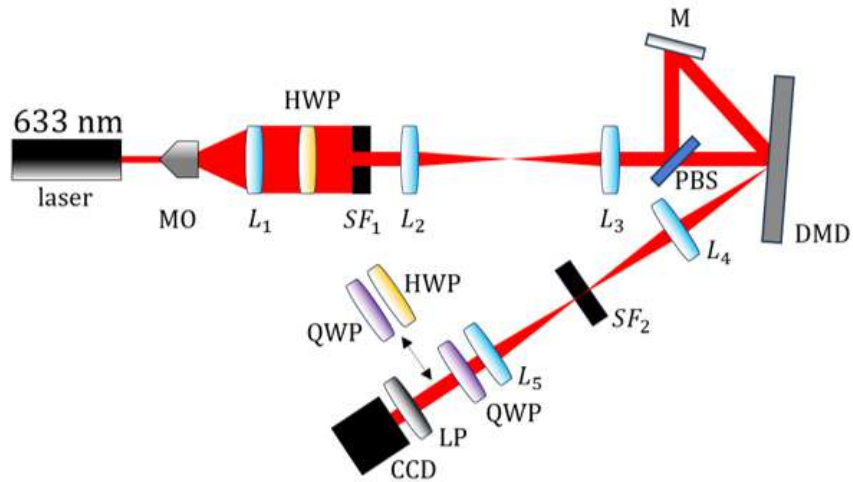
Figure 2.12: Schematic representation of the experimental setup with a polarizing beam splitter.

Vector beams of different families were generated with this experimental set-up. In Figure 2.13 the corresponding intensity profiles (R, L, H and D) were captured and contrasted with the simulated predictions for a) LGVB$(1,0)$ with $\theta = \pi/4$ and $\delta = \pi/2$, b) LGVB$(1,0)$ with $\theta = \pi/4$ and $\delta = 0$, c) HIGVB$(3,5)$ with $\theta = \pi/4$ and $\delta = \pi$ d) MGVB$(4,4)$ with $\theta = \pi/4$ and $\delta = 0$.
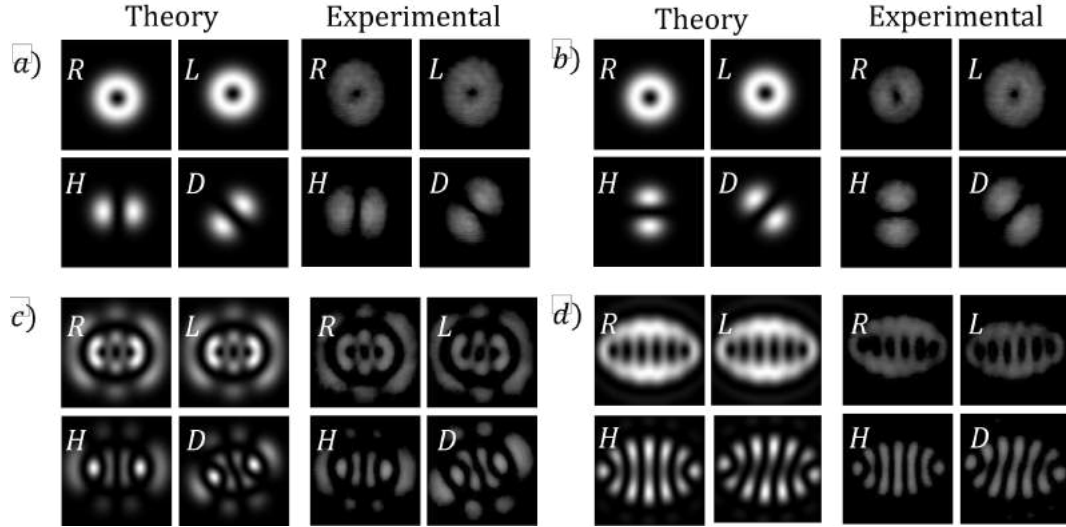
Figure 2.13: Vector Beam intensity distributions in its polarization projections. A theoretical intensity distributions in its polarization projections of a) LGVB$(1,0)$ with $\theta = \pi/4$, $\delta = 0$ and $W_0 = 0.5$, b) LGVB$(1,0)$ with $\theta = \pi/4$, $\delta = \pi/2$ and $W_0 = 0.5$, c) HIGVB$(3,5)$ with $\theta = \pi/4, \delta = \pi$, $W_0 = 0.5$ and $e = 2$ d) HMGVB$(6,6)$ with $\theta = \pi/4, \delta = 0$, $W_0 = 1.0$, $e = 0.8, a = 1, k_t = 10$, $z = 0$ with its experimental measurements. R and L represent the intensity distribution in its right and left circular polarization projection, respectively. H and D are the intensity distributions in its horizontal and diagonal projection. ($\lambda = 633$ nm)
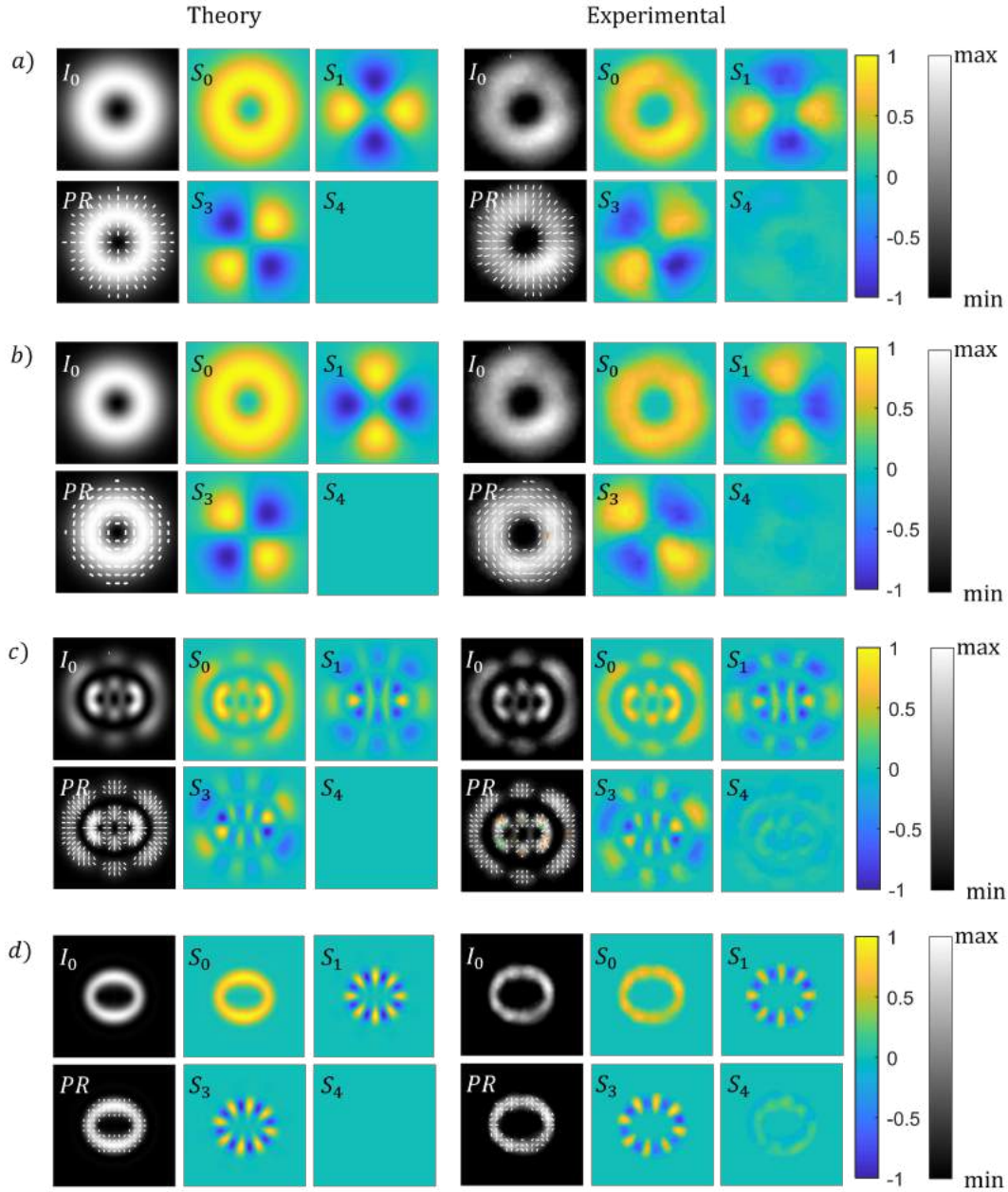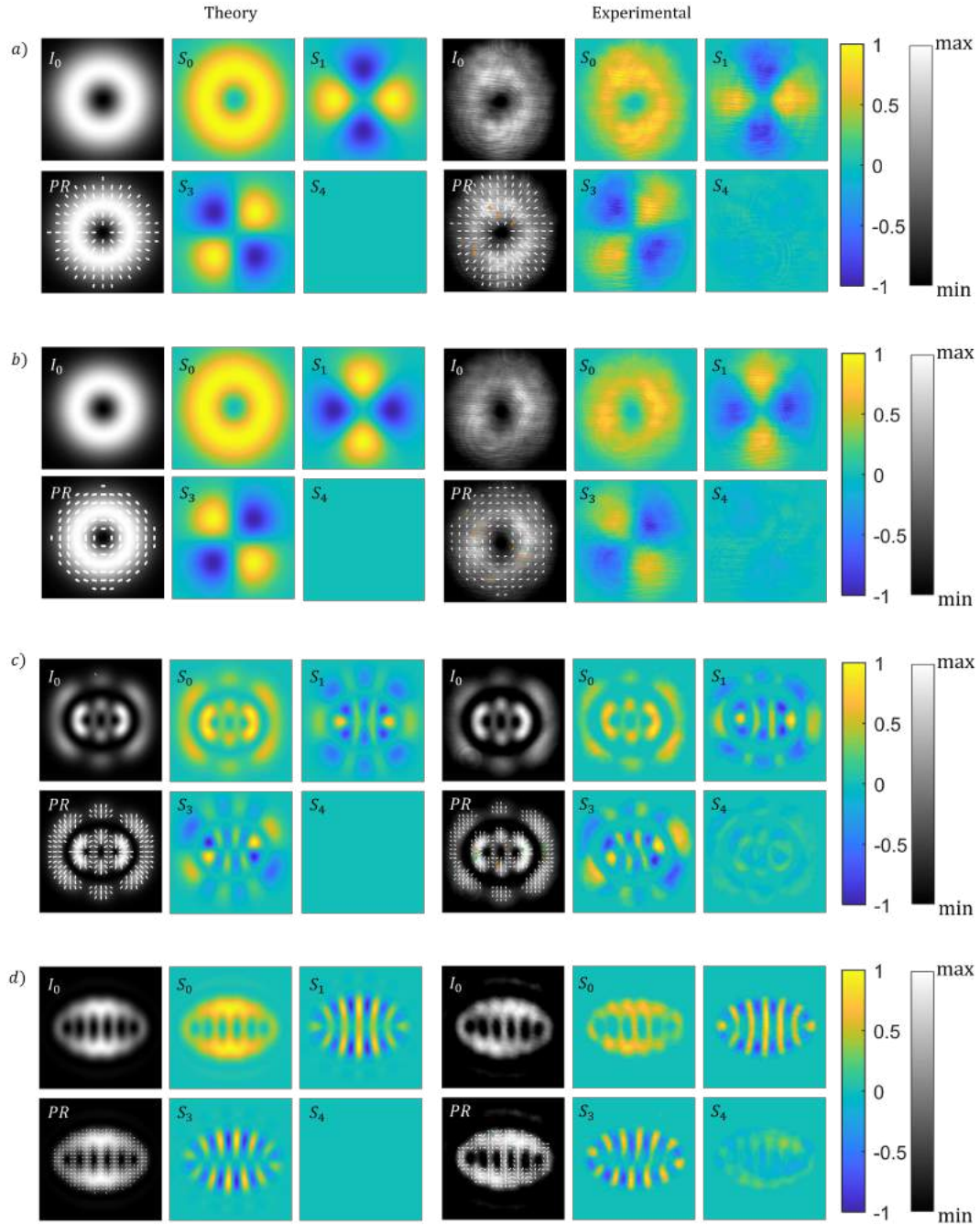
Figure 2.14: Stokes parameters of Vector Beams. A contrast between a theoretical a) LGVB$(1,0)$ with $\theta = \pi/4$, $\delta = 0$ and $W_0 = 0.5$, b) LGVB$(1,0)$ with $\theta = \pi/4$, $\delta = \pi/2$ and $W_0 = 0.5$, c) HIGVB$(3,5)$ with $\theta = \pi/4$, $\delta = \pi$, $W_0 = 0.5$ and $e = 2$ d) HMGVB$(6,6)$ with $\theta = \pi/4$, $\delta = 0$, $W_0 = 1.0$, $e = 0.8$, $a = 1$, $k_t = 10$, $z = 0$ and its experimental Stokes polarization reconstruction. I_0 represent the intensity of the vector mode, S_0, S_1, S_2 and S_3 represent the intensity for each Stokes parameter and PR is the polarization reconstruction of the vector beam. ($\lambda = 633nm$)

Their corresponding Stokes parameters calculated with this intensity profiles were

determined and are presented in Figure 2.14. As we can see there is a very good agreement with theoretical predictions given by the numerical simulations. Also, the state of PR has a high fidelity between the calculated and the theoretical expected.

Chapter 3

Partially Coherent Vector Beams

In this section we present a generalization of the work proposed in [3, 14] where the authors discuss the generation of scalar partially coherent beam by a incoherent superposition of multiple displaced beams in a given region. These works are relevant since they are the first to show an experimental technique that provides control over the beam transversal coherence length unlike other experimental designs. In addition to that, they study their cross-correlation function which shows very good agreement with the numerical simulations. That is why, for the purposes of this work, his proposal for the generation of partially coherent scalar beams has been taken and has been generalized for vector beams. In order to generate a partial spatial coherent beam, the concept of partial coherence should be understand as the deterioration of interference fringe visibility because of the effects of an extended source size where each point on the source produce an interference pattern which is shifted with respect to the others and they are incoherently superimposed.

3.1   Description of a partially coherent vector beam

In this work we generalize the proposed in some articles [3, 14] but for vector beams. In this way, to describe a spatially partially coherent beam we require to generate a incoherent superposition of N randomly displaced vector beams $\vec{u}_l(x, y)$ on the xy plane with random phases across the transversal plane. The location of each individual beam is arranged such that the beams are uniformly distributed at random positions given by coordinates (a_j, b_j) that are random numbers uniformly distributed within a circular region of radius c. An schematic representation of the superposition

is on Figure 3.1. The general expression for a vector beam is then

$$\vec{E}_k(x,y) = \sum_{j=0}^{N} \vec{u}_l(x - a_j, x - b_j) \exp(i\phi_j) \tag{3.1}$$

where $\vec{u}_l(x,y)$ can be any vector beam mode but only in the appropriate coordinate system. As we can see in equation 3.1, each vector beam is multiplied by a random phase term $\exp(i\phi_j)$ in which ϕ_j is randomly distributed between 0 and 2π. The locations inside the circle obtained using the **Algorithm 1**. This new part of algorithm is going to be added to the previous ones to generate the partially coherent vector beams.
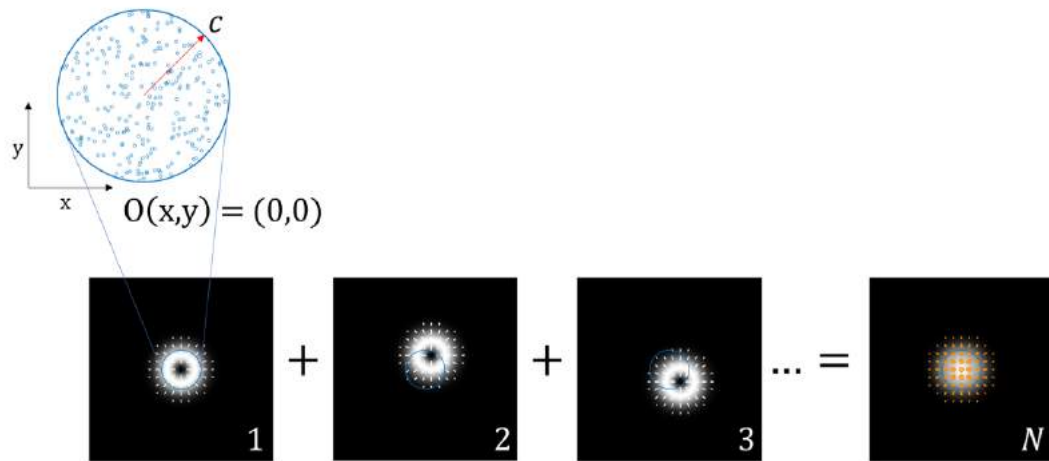
Figure 3.1: Schematic representation of the intensity resulting from the coherent superposition of N-vector beams with centers randomly displaced within a circular region of radius c to create a partially coherent vector beam.

In **Algorithm 1**

(a) Line 2: N is the number of positions desired inside the circle

(b) Line 3: c is the radius of the circle

(c) Line 4: Usually, the coordinates of the center of the circle are chosen in the origin, $(0,0)$. However, experimentally this could change depending on where the beam hits the light modulator, which is why they are left free to choose.

(d) Line 5: rand$(1, N)$ returns a $1 \times N$ array of uniformly distributed random numbers.

Algorithm 1 Random positions in a circle. The function receives N number of desired positions inside a circle of radius c with origin $0(h, k)$ and generates N points random uniformly distributed inside it.

1: **procedure** RANDOMPOSITIONCIRCLE(N, c, h, k)
2:     N ▷ Number of positions in a circle
3:     c ▷ Radius
4:     $O(h, k)$ ▷ Coordinates of the center
5:     $\theta \leftarrow 2\pi \text{rand}(1, N)$
6:     $r \leftarrow c\sqrt{\text{rand}(1, N)}$
7:     $x_0 \leftarrow h + r\cos\theta$
8:     $y_0 \leftarrow k + r\sin\theta$
9: **end procedure**

   (e) Line 7 and Line 8: The new coordinates correspond to each point generated and they are calculated by adding the original center (h, k) plus the correspondent component of the vector, r.

3.2 Partial degree of polarization in a vector beam

As we see in Section 2, a general vector mode can be written as

$$\mathbf{E}(r, \theta) = \alpha V(r, \theta)^- \hat{e}_L + \beta V(r, \theta)^+ \hat{e}_R \tag{3.2}$$

where E_R and E_L are the orthogonal components of the field and $|a|^2 + |\beta|^2 = 1$. In particular a displaced version of a vector vortex mode can be expressed as

$$\mathbf{E}(r, \theta) = \alpha[r\exp(-i\theta) - \rho\exp(-i\phi)]\hat{e}_L + \beta[r\exp(i\theta) - \rho\exp(i\phi)]\hat{e}_R \tag{3.3}$$

The average of the Stokes parameters over many realizations is

$$S_0(r, \theta) = \langle |E_R(r, \theta)|^2 + |E_L(r, \theta)|^2 \rangle \tag{3.4a}$$

$$S_1(r, \theta) = \langle 2\,\text{Re}\{E_R^*(r, \theta)E_L(r, \theta)\} \rangle \tag{3.4b}$$

$$S_2(r, \theta) = \langle 2\,\text{Im}\{E_R^*(r, \theta)E_L(r, \theta)\} \rangle \tag{3.4c}$$

$$S_3(r, \theta) = \langle |E_R(r, \theta)|^2 \langle - \rangle |E_L(r, \theta)|^2 \rangle \tag{3.4d}$$

The term $\langle |E_L|^2 \rangle$ present in the previous equations is

$$\langle |E_L|^2 \rangle = |\alpha| \langle r^2 + \rho^2 - 2r\rho \cos\theta \cos\phi + 2r\rho \sin\theta \sin\phi \rangle, \tag{3.5a}$$

$$= |\alpha|^2 (r + \langle \rho^2 \rangle - 2r\cos\theta \langle \rho \cos\phi \rangle - 2r\sin\theta \langle \rho \sin\phi \rangle) \tag{3.5b}$$

Consider the random variables W $Uniform(0,1)$ and Φ $Uniform(0, 2\pi)$, then we perform the following transformation

$$R = c\sqrt{W} \tag{3.6}$$

so that ρ R. By applying the mapping in eq. 3.6, we obtain

$$\langle |E_L(r,\theta)|^2 \rangle = |\alpha|^2 (r^2 + \frac{1}{2}c^2) \tag{3.7}$$

where $c > 0$ represents the radius of a circular region where many randomly displaced vortices are located. Following the same procedure we can find E_R

$$\langle |E_R(r,\theta)|^2 \rangle = |\beta|^2 (r^2 + \frac{1}{2}c^2) \tag{3.8}$$

With eqs. 3.7 and 3.8 we can calculate $S_0(r,\theta)$ and $S_3(r,\theta)$. Now, obtaining S_1

$$S_1(r,\theta) = \langle 2\,\mathrm{Re}\{E_R^*(r,\theta)E_L(r,\theta)\}\rangle, \tag{3.9a}$$

$$= 2\alpha\beta^* \langle \mathrm{Re}\{r^2 \exp(-i2\theta) - 2r\rho \exp(-i(\theta+\phi)) + \rho^2 \exp(-i2\rho)\}\rangle, \tag{3.9b}$$

$$= 2\alpha\beta^* (r^2 \cos 2\theta + 4\langle \rho^2 \cos 2\phi \rangle - 2r\langle \cos(\theta - \phi) \rangle) \tag{3.9c}$$

$$= 2\alpha\beta^* r^2 \cos 2\theta \tag{3.9d}$$

In the same way, $S_2(r,\theta)$ can be obtained

$$S_2(r,\theta) = -2\alpha\beta^* r^2 \sin 2\theta \tag{3.10}$$

Summarizing the results of the Stokes parameters

$$S_0(r,\theta) = r^2 + \frac{1}{2}c^2 \tag{3.11a}$$

$$S_1(r,\theta) = 2\alpha\beta^* r^2 \cos 2\theta \tag{3.11b}$$

$$S_2(r,\theta) = -2\alpha\beta^* r^2 \sin 2\theta \tag{3.11c}$$

$$S_3(r,\theta) = (|\alpha|^2 - |\beta|^2)(r^2 + \frac{1}{2}c^2) \tag{3.11d}$$

The degree of polarization is then calculate as

$$P(r,\theta) = \frac{\sqrt{S_1^2 + S_2^2 + S_3^2}}{S_0} \tag{3.12a}$$

$$= \sqrt{\frac{4(\alpha\beta^*)^2 r^4}{(r^2 + \frac{1}{2}c^2)^2} + (|\alpha|^2 - |\beta|^2)^2} \tag{3.12b}$$

In the eq. 3.12, as c approaches to zero, the degree of polarization tends to 1. On the other hand, as c increases, the degree of polarization is not uniform across the transverse plane. when $c > 0$, the degree of polarization also tends to 1 as the readial coordinate increases. The lowest degree of polarization is $|\alpha|^2 - |\beta|^2$ which is in the central point of the vector vortex beam.

3.3 Generation of partially coherent vector beam

To generate a PCVB, we employed the experimental set-up shown in Figure 2.9 and Figure 2.12 both with a DMD displaying a movie at 60Hz. Each frame of the movie contains a different multiplexed hologram slightly displace from the center generated in a previous process before sending them to the DMD. Unfortunately, the experimental generation cannot be completed due to diverse technical limitations. At the beginning we start working with the experimental set-up that has a common-path interferometer shown in Figure 2.9 but we notice that, when the beam is divided by the PBS. each of the orthogonal components of the vector beam acquired different phases that we associate with factors such as atmospherical turbulence, temperature, suspended particles, among other, so that the associated electric fields oscillated with an unknown phase shift and, when both orthogonal components are multiplexed at the end of the interferometer,they turned out to be relevant when generating partially coherent vector beams. With this analysis we proceed to use the technique shown in Figure 2.12. This experimental set-up has the property that the division of the beam in its orthogonal polarization components is before it is modulated by the DMD so at the output of the DMD we already have a vector beam on axis so the problem with the extra phase shifts does not exist. However, some technical problems persisted such as the camera's frames per second capture speed that did not allow real-time capture of the partially coherent vector beam, the loss of speed due to communication between the computer, the DMD and the camera mainly with the number of frames per second sent in the video by the computer, received by the DMD and captured by the camera.

However, numerical simulations of PCVBs could be carried out. As we mention previously, we add the **Algorithm 1** to the **Algorithm 2** in order to be able to do the coherent sum and generate the intensity profile of partially coherent vector beam.

Basically, at the end of the **Algorithm 5** we are going to have $N + 1$ images but we only considered two main images: The N-Stokes parameters image and the intensity and polarization distribution image as we can see in Figure 3.2.
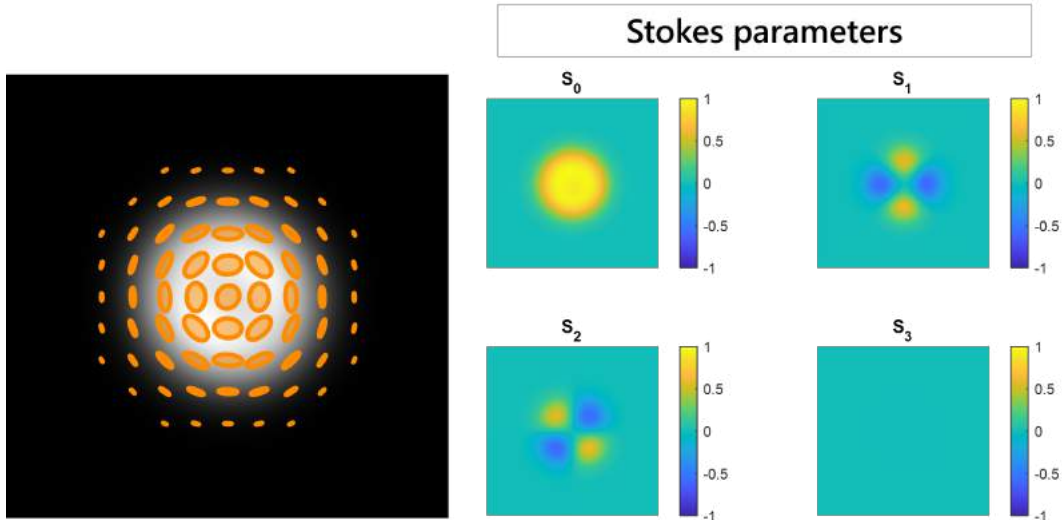
Figure 3.2: Example of two images obtained by the **Algorithm 5**. A 250 $LG(1,0)$ vectorial beams superposed in a circle of radius, $c = 0.4$.

Some particular cases will be shown for each of the families of interest in this work: Laguerre-, Helical Ince- and Helical Mathieu-Gaussian. In the examples, we are going to set the number of superposed beams to 200 so we are only to change the radius, c.
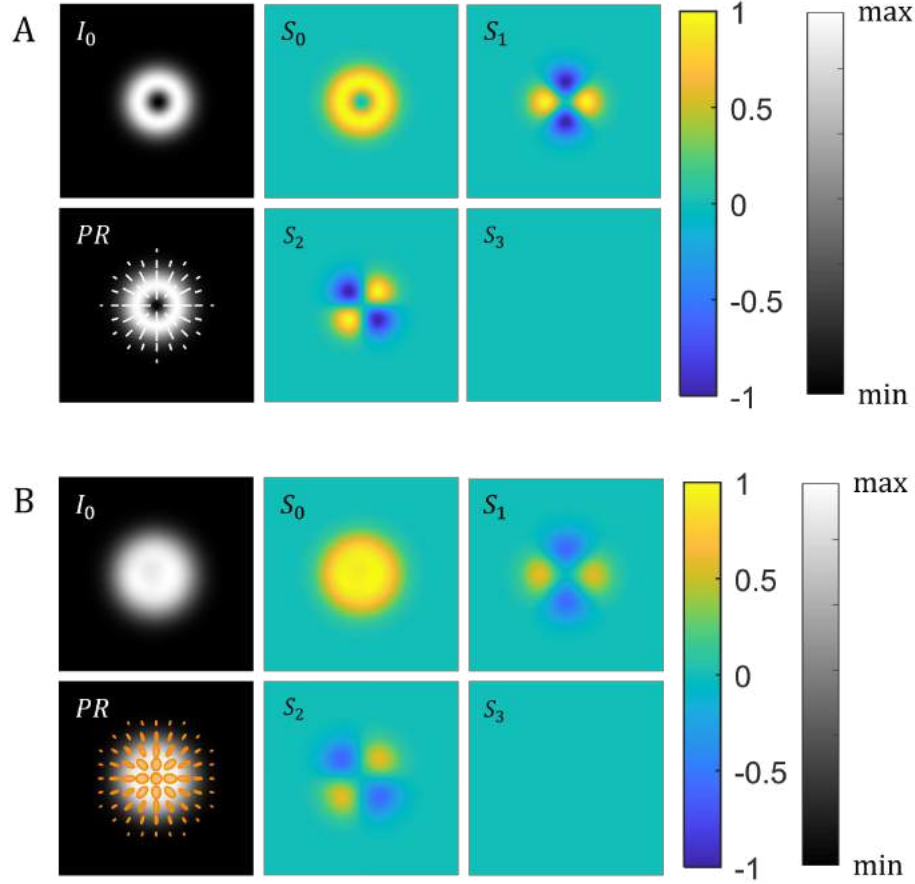
Figure 3.3: LG Fully Coherent Vector Beam vs LG Partially Coherent Vector Beam. A) LG(1, 0) with $\alpha = \pi/4$ and $\theta = 0$. B) LG(1, 0) with $\alpha = \pi/4$, $\theta = 0$ with radius $c = 0.5$. I_0 represent the intensity of the vector mode, S_0, S_1, S_2 and S_3 represent the intensity for each Stokes parameter and PR is the polarization reconstruction of the vectorial beam. ($\lambda = 633nm$, $W_0 = 0.6$, $z = 0.1$)

In Figure 3.3 a comparison between a fully HLG coherent vector beam and a **Partially Coherent Helical Laguerre-Gaussian Vector Beam (PCHLGVB)** is presented with the Stokes parameters include. We can see in the distribution of intensity in PCHLGVB, the dark core in the center of the beams is filled with diffused light and it becomes difficult to distinguish it. The distribution of polarization remains the same but the polarization states at each point of the intensity profile changes. Instead of having only linear polarization, circular and elliptical states of polarization are observed as result of the average of the multiple linear directions of the superimposed beams.
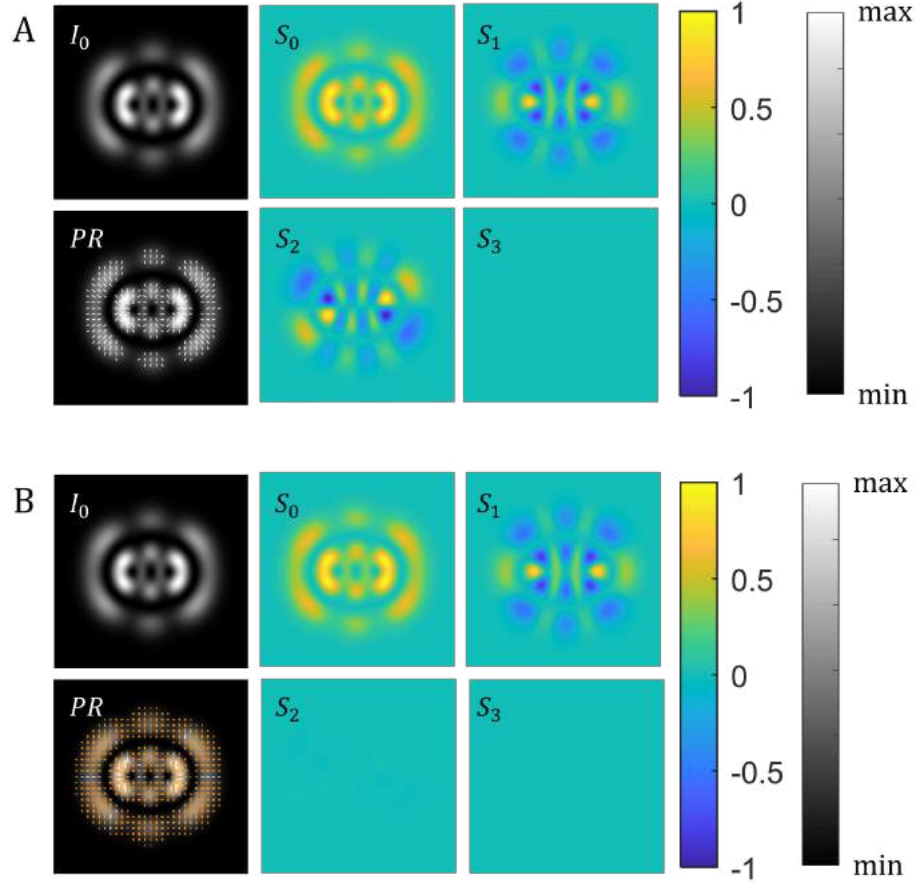
Figure 3.4: HIG Fully Coherent Vector Beam vs. HIG Partially Coherent Vector Beam. A) HIG$(3,5)$ with $\alpha = \pi/4$ and $\theta = 0$. B) HIG$(3,5)$ with $\alpha = \pi/4$, $\theta = 0$ and radius $c = 0.5$. I_0 represent the intensity of the vector mode, S_0, S_1, S_2 and S_3 represent the intensity for each Stokes parameter and PR is the polarization reconstruction of the vectorial beam. ($\lambda = 633nm$, $W_0 = 0.6$, $e = 2$

Partially Coherent Helical Ince-Gaussian Vector Beam (PCHIGVB) is shown at the bottom of Figure 3.4. In comparison with its fully coherent version, the dark holes and the structure of the beam in general becomes diffused. In contrast with PCLGVB, in the PCHIGVB the distribution of polarization does not remain the same and the presence of linear, elliptical and circular states of polarization appears for the same reason.

Finally, for **Partially Coherent Helical Mathieu-Gaussian Vector Beam (PCHMGVB)** in Figure 3.5, the dark structures also are filled with diffused light and the borders becomes less sharp. Like the PCHIGVB, the PCHMGVB do not maintain their polarization distribution and they present linear, elliptical and circular polarization states in their profile.
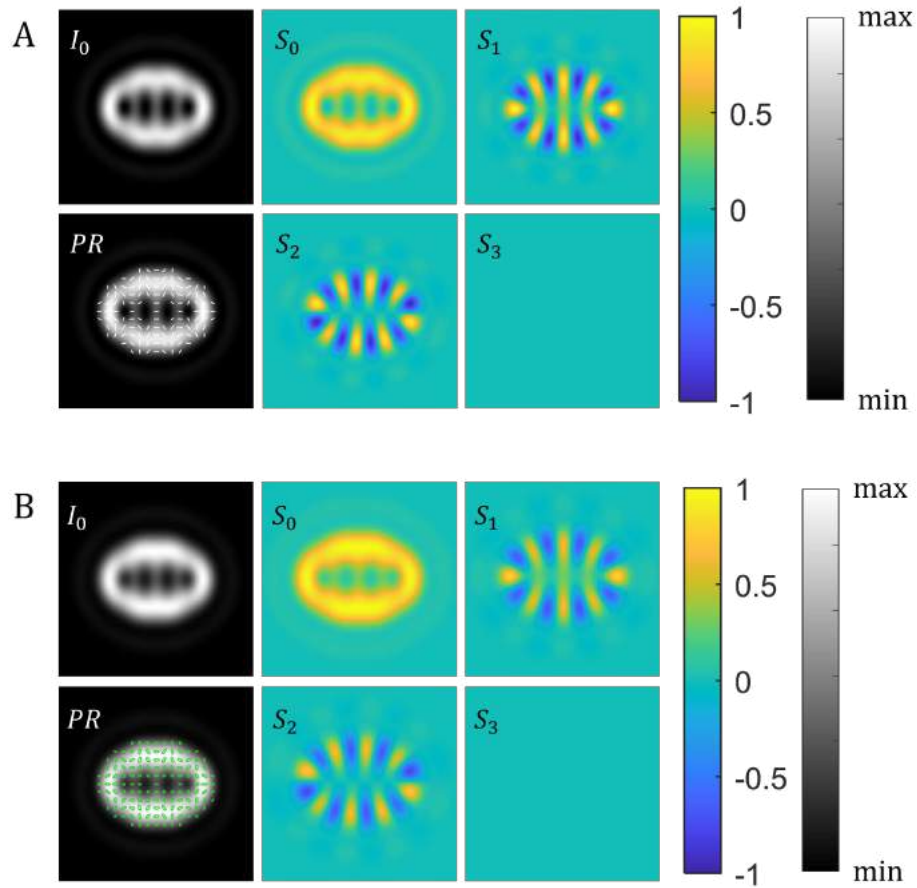
Figure 3.5: HMG Fully Coherent Vector Beam vs. HMG Partially Coherent Vector Beam. A) HMG$(4,4)$ with $\theta = \pi/4$ and $\delta = \pi$. B) HIG$(3,5)$ with $\theta = \pi/4$, $\delta = \pi$ and radius $c = 5$. I_0 represent the intensity of the vector mode, S_0, S_1, S_2 and S_3 represent the intensity for each Stokes parameter and PR is the polarization reconstruction of the vectorial beam. $(\lambda = 633nm$, $k_t = 1$, $e = 0.2, a = 1$
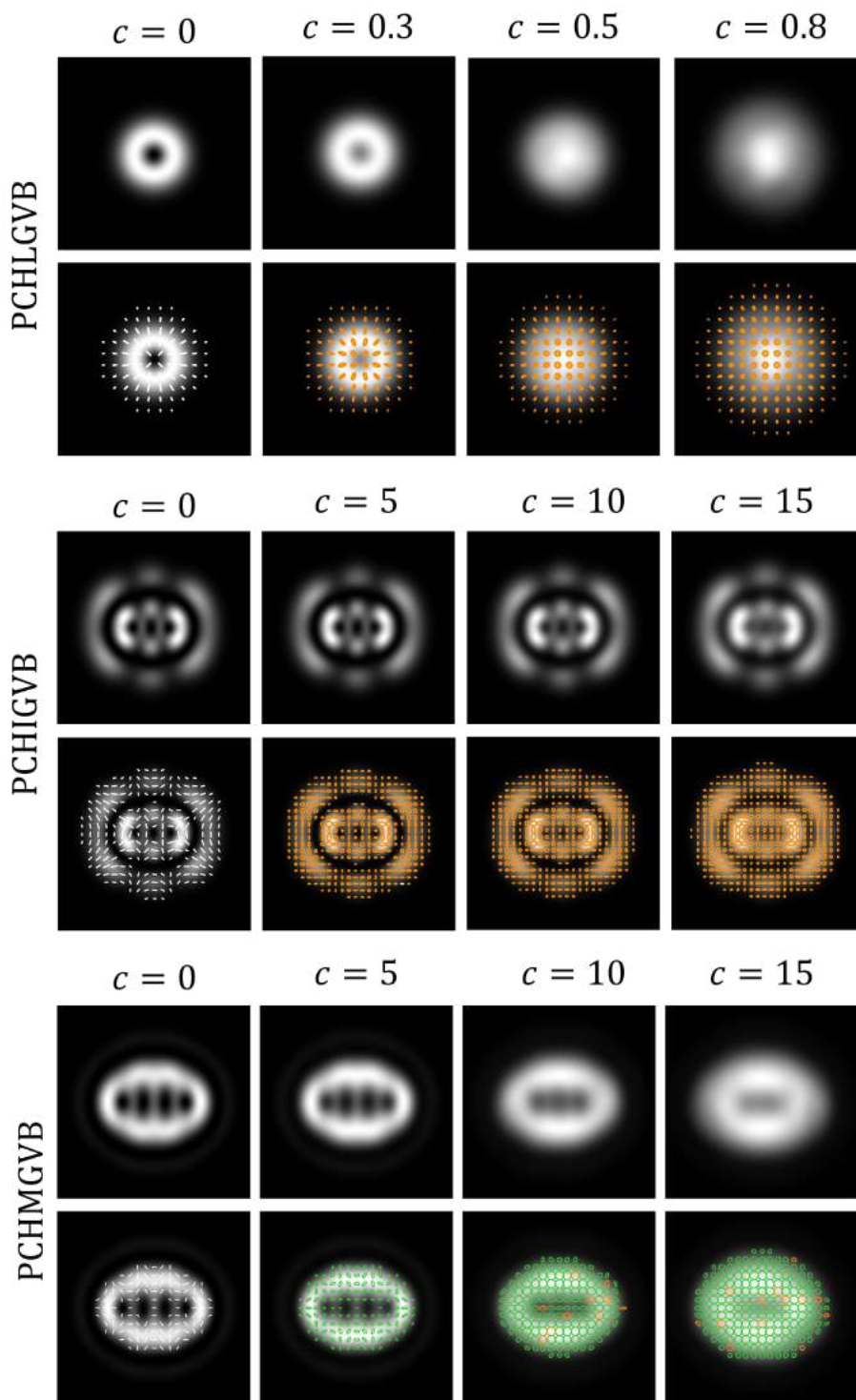
Figure 3.6: Comparison between different families of beams in partially coherent regime.

In Figure 3.6 we can see the three families studied in this thesis: **HLG**, **HIG** and **HMG**. The coherence of these beams degrades as the radius c changes, starting from

complete coherence when $c = 0$. It can be seen that for the PCHLGVB, the coherence is easily lost with radii that are not very large in comparison with PCHIGVB and PCHMGVB. In the case of PCHIGVB, the spatial mode is more preserved compared to the other two families even when the value of the radius is increased and the polarization distribution as well as the polarization states present undergo barely noticeable changes.

Chapter 4

Conclusion

The versatility of structured light promises a future where it has multiple applications. This versatility is due to the manipulation of its properties and degrees of freedom: spatial, polarization, temporal, wavelength, and others. In this thesis we have also explored the partial spatial coherence of a structured beam with the intention of contributing to the generation of partially coherent vector beams. In Chapter 1 we discuss the basis theory that supports structured light. We started by deriving the Helmholtz paraxial wave equation by assuming that a paraxial light beam is formed mainly of plane waves that are paraxial to the propagation direction of the beam so the wave vector $\mathbf{k}$ lies along the propagation axis. A partial differential equation for the amplitude distribution can be found where if the profile is slowly varying with the propagation axis, the second derivative is much smaller than the first one multiplied by the wave number and simultaneously, the transverse variation is larger than the second derivative. This paraxial approximation can hold solutions in different coordinate system some of which are presented in this thesis, namely,as Laguerre-Gaussian in cylindrical coordinates and Ince-Gaussian in elliptic coordinates. We also present Mathieu-Gaussian which is a solution but to the Helmholtz equation in elliptical cylindrical coordinates. We outlined a description of polarisation, a manifestation of the vector nature of light. We also outlined its matricial formalism in terms of Jones matrices. Finally, we also described its geometrical representation in the so-called Poincaré sphere. The Stokes parameters are also presented in this chapter because unlike the ellipse of polarization, they allow to describe polarized, partially polarized and unpolarized light so it can be said they are more general. More importantly, Stokes parameters provide a way to measure experimentally the different states of polarisation. Here is shown the conventional technique to do Stokes polarimetry measuring only four intensities with the aim of a polarization state analyzer and a

CCD camera. As we mention previously, the coherence is one of the main topics in this thesis so in this chapter the unified theory of coherence and polarization where we redefine the polarization properties of a partially coherent vector beam with the generalized Stokes parameters and the spectral degree of polarization. Finally, at the end of this chapter, we reviewed the Spatial Light Modulator and the Digital Micro-Mirror Device as a techniques in which structured light beams can be generated.

In Chapter 2 we delved into the main features of vector beams: the weighting factors and the intermodal and intramodal phase. The weighting factors or amplitude modify the polarization ellipses in the polarization distribution passing from scalar beams with homogeneous circular polarization to vector beams with elliptical and liner polarization. The intramodal phase is associated with the components of the helical mode and the intermodal phase is the difference between the polarization components of the spatial modes. These properties generate different vector beams that can be organized in the High Order Poincaré Sphere where if we vary the value of θ or by modulating the weight factors, the polarization can be transformed along the longitudes on the HOPS for the northern hemisphere to the southern hemisphere, going from beams circularly polarized scalars, passing through elliptical states until reaching the equator where linearly polarized beams meet. On the other hand, if the intermodal phase is modified, each of the polarization ellipses distributed in the beam polarization profile rotates in such a way that it can be said that by changing the angle δ, an azimuth displacement is obtained. In this chapter we discuss the condition that converts the solution families previously shown into to helical that is basically a linear combination of even and odd beams. We demonstrated this helical vector beams experimentally using two different setup and reinforced our observation with theoretical simulations that shows very good agreement in both cases.

In Chapter 3 we have introduced partially coherent vector beams (PCVBs) as a generalization of the scalar case [3, 14]. The proposal consists in generate a coherent superposition of N randomly uniform displaced vector beams on the xy plane with random phases across the transversal plane. We carried out two experiments to show the generation of spatially partially coherent vector beams using only a DMD as a digital means for their construction with this technique the aim was to have control over the degree of coherence. Unfortunately, due to technical limitations we cannot be able to generate them. The incorporation of high-speed digital cameras and spatial light phase modulators as well as electromechanical devices for wave plate retarders rotation to take the four intensity measurements to do Stokes polarimetry in the discussed experimental set-ups will further increase the benefits of these techniques.

However, numerical simulations of PCVBs could be carried out to show the behaviour of these kind of beams. We observe that the dark holes and the structure of the beam in general becomes diffuse as the radius c increases, the ellipses of polarization distributed in the profile of polarization changes so we have the presence of different types of ellipses in the same vector beam. For Partially Coherent Helical Laguerre-Gaussian Vector Beams the polarization distribution persists and this is only observed in vortex beams.

As future work, it remains to improve the technique of experimental generation of PCVBs as well as their formal characterization. The stability of the beams is a general problem in structured light, which is why work has been carried out on the proposal to generate on-axis vector beams, that is, in the experiment the beam is not split into two to manipulate them independently, rather, we take advantage of the polarisation-sensitive of SLMs to manipulate both degrees of freedom in an on-axis configuration. This proposal includes the combination of two techniques: complex amplitude modulation to obtain scalar beams and on-axis modulation to generate vector beams. This work can is in the final stage prior to its publication in Journal of Optics and is entitled *"Generation of super-stable vector modes using on-axis complex-amplitude modulation"*. As a final comment, to improve the speed of communication between the computer and the DMD, it is proposed to consider recording the hologram movie in the internal memory of the DMD or using techniques such as high speed, complex wavefront shaping [48]. On the other hand, the characterization of the PCVBs obtained includes advanced knowledge in statistical optics that allows them to be modelled and thus, to find useful parameters such as determining the number of superimposed vector beams that are required for a certain degree of partial coherence.

Appendix A

Algorithms

In this section we present a general algorithms to generate a vector beam and to characterize them using the Stokes parameters.

Some comments about the algorithm 2 are

(a) Line 2 and Line 3: H and V are considered to be equal magnitude in order to obtain a square image and prevent the intensity of the mode from being distorted.

(b) Line 6: $pxSize$ is considered 5.4×10^{-6}m because it is the size of the pixel in the Light modulator that we are planning to use in the experimental phase of future work

(c) Line 13 and Line 14: p and m are only examples of indices and degrees of the polynomial, some families are going to have more parameters

(d) Line 17 and Line 18: The function BeamFunction corresponds to the family of beams to be generated. In general, the function has at least exposed input values. However, it might require more depending on the complexity of the family polynomial it describes.

(e) Line 19 and Line 20: The two orthogonal scalar fields with scalar polarization from equation 2.2 are described here.

The algorithm 2 generates two images that are shown in Figure A.1, the first one is the intensity of the mode and the second one is a mosaic that includes the projections in each one of the directions. To visualize the intensity profile in Stokes parameters, the algorithm 3 must be implemented. About the algorithm 3

(a) Line 2 to Line 5:The division by $\max(I_0)$ is in order to normalize the values.

Algorithm 2 Generation of a vector mode.

1: **procedure** INTENSITYVECTORMODE($H, V, pxSize, \lambda, W_0, m, p, \alpha, \delta$)
2:     H ▷ Horizontal image size in pixels
3:     V ▷ Vertical image size in pixels
4:     $x \leftarrow \text{linspace}(-(H/2), (H/2) - 1, H)$
5:     $y \leftarrow \text{linspace}(-(V/2), (V/2) - 1, V)$
6:     $pxSize$ ▷ Pixel size to scale the image
7:     $x \leftarrow x \cdot pxSize$
8:     $y \leftarrow y \cdot pxSize$
9:     $[X, Y] \leftarrow \text{meshgrid}(x, y)$
10:     λ ▷ Wavelenght
11:     W_0 ▷ Waist radius
12:     z ▷ Direction of wave traveling
13:     m ▷ Indice
14:     p ▷ Indice
15:     α ▷ Weight factor (0 to $\pi/2$)
16:     δ ▷ Intermodal phase (0 to π)
17:     $u_1 \leftarrow \text{BeamFunction}(H, V, x, y, even, m, p, W_0, \lambda, z)$
18:     $u_2 \leftarrow \text{BeamFunction}(H, V, x, y, odd, m, p, W_0, \lambda, z)$
19:     $E_R = \cos\alpha \cdot u_1$
20:     $E_L = \exp(i\delta) \sin\alpha \cdot u_2$
21:     $E_H = (E_L + E_R)/\sqrt{2}$
22:     $E_D = (E_H + E_V)/2$
23:     $I_L = E_L \cdot E_L^*$
24:     $I_R = E_R \cdot E_R^*$
25:     $I_H = E_H \cdot E_H^*$
26:     $I_D = E_D \cdot E_D^*$
27:     $I_0 = I_L + I_R$
28: **return** I_L, I_R, I_H, I_D, I_0
29: **end procedure**
30: **figure**
31: $\text{image}(I_0), \text{title}('Intensity')$
32: **figure**
33: $\text{subplot}(2, 2, 1), \text{image}(I_L), \text{title}(I_L)$
34: $\text{subplot}(2, 2, 2), \text{image}(I_R), \text{title}(I_R)$
35: $\text{subplot}(2, 2, 3), \text{image}(I_H), \text{title}(I_H)$
36: $\text{subplot}(2, 2, 4), \text{image}(I_D), \text{title}(I_D)$
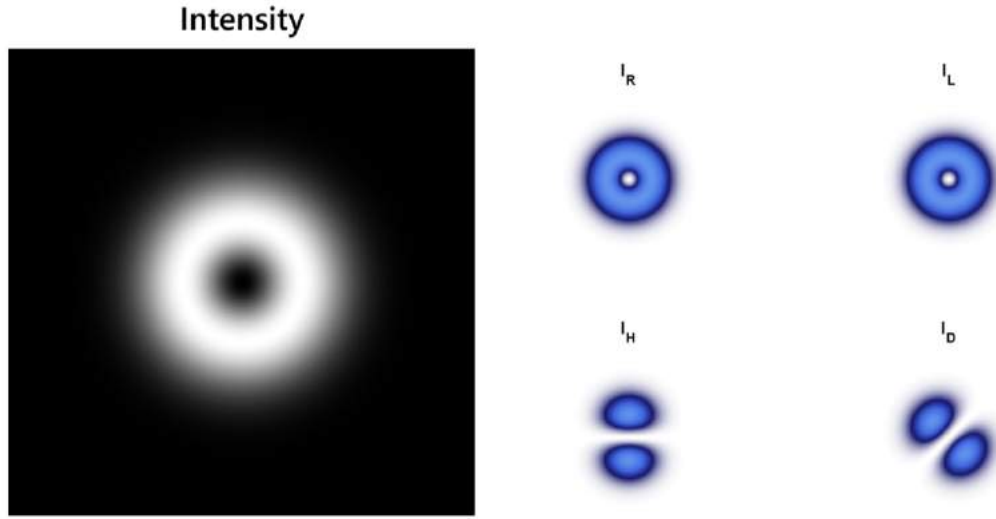
Figure A.1: The figures generated by the algorithm 2. On the left we have the intensity of the vector mode of a $LG(1,0)$ with $\alpha = \pi/4$ and $theta = \pi/2$ and the figure at the right is a mosaic with the projections of intensity in each direction

---

Algorithm 3 Stokes Parameters

1: **procedure** STOKESPARAMETERS(I_L, I_R, I_H, I_D, I_0)
2:     $S_0 \leftarrow I_0/\max(I_0)$
3:     $S_1 \leftarrow (2I_H - S_0)/\max(I_0)$
4:     $S_2 \leftarrow (2I_D - S_0)/\max(I_0)$
5:     $S_3 \leftarrow (2I_R - S_0)/\max(I_0)$
6: **return** S_0, S_1, S_2, S_3
7: **end procedure**
8: **figure**
9: subplot$(2, 2, 1)$, image$(S_0, [-1, 1])$, title(S_0)
10: subplot$(2, 2, 2)$, image$(S_1, [-1, 1])$, title(S_1)
11: subplot$(2, 2, 3)$, image$(S_2, [-1, 1])$, title(S_2)
12: subplot$(2, 2, 4)$, image$(S_3, [-1, 1])$, title(S_3)
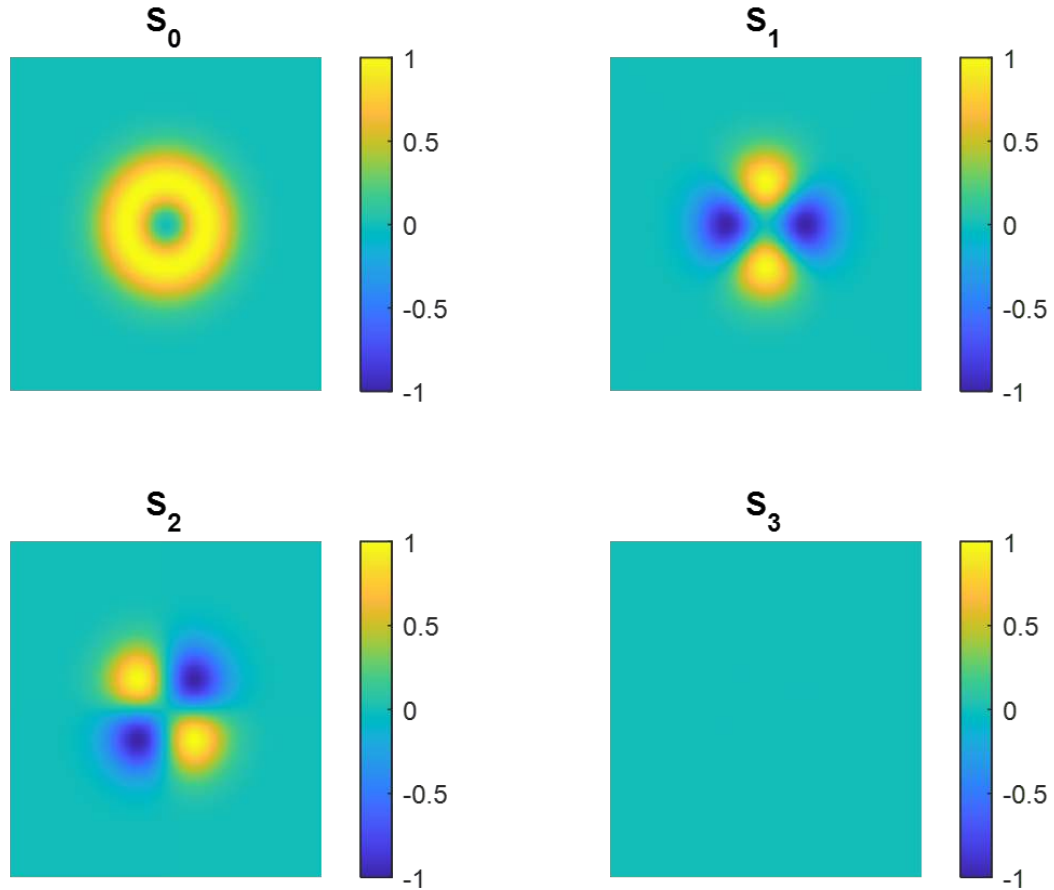
Figure A.2: Figure generated by the algorithm 3 which is a mosaic that includes all the four Stokes parameters of a LG(1,0) with $\alpha = \pi/4$ and $theta = \pi/2$

(b) Line 9 to Line 12: The values $[-1, 1]$ are the range of values admitted in the scaled image because are only those who had a physical meaning.

With the Stokes Parameters algorithm we obtain a mosaic image like shown in Figure A.2 with the four Stokes parameters that help us to know the characteristics of the beam. The first image in the mosaic, which is S_0 describes the total intensity of the optical beam; the second image is S_1 which tells us the preponderance of light horizontally polarized over light vertically polarized; the third image and parameter S_2 shows us the preponderance of light polarized at $+45\,\mathrm{deg}$ over light polarized $-45\,\mathrm{deg}$ and, finally, S_3 describes the preponderance of right circularly polarized light over left circularly polarized light [49].

To visualize the distribution of the polarization over the intensity profile, we must add to the sequence the algorithm 4. The algorithm uses the previous values returned in the algorithm 3 to, basically calculate the polarization ellipse at each point on the

---

Algorithm 4 Stokes

1: **procedure** STOKESELLIPSES($S_0, S_1, S_2, S_3, n, le, cmap$)
2:    N ▷ Image resolution
3:    le ▷ Ellipse size
4:    cmap   ▷ Matrix of colors for different orientation polarization ellipses
5:    $S_0 \leftarrow \sqrt{S_1^2 + S_2^2 + S_3^2}$
6:    $samp \leftarrow N/10$
7:    $L \leftarrow \sqrt{S_1^2 + S_2^2}$
8:    $a \leftarrow \mathrm{Re}\left\{\sqrt{\frac{S_0+L}{2}}\right\}$ ▷ Semi major axis
9:    $b \leftarrow \mathrm{Re}\left\{\sqrt{\frac{S_0-L}{2}}\right\}$ ▷ Semi minor axis
10:    $\phi \leftarrow \mathrm{angle}(S_1 + i \cdot S_2)/2$ ▷ Rotation angle
11:    $h \leftarrow \mathrm{sign}(S_3)$ ▷ Handedness
12:    $ip \leftarrow \mathrm{round}(\mathrm{linspace}(1, \mathrm{length}(S_0), samp))$
13:    $a_1 \leftarrow a(ip, ip) \cdot le$
14:    $b_1 \leftarrow b(ip, ip) \cdot le$
15:    $hp_1 \leftarrow h(ip, ip)$
16:    $\phi_1 \leftarrow \phi(ip, ip)$
17:    $S_{01} \leftarrow S_0(ip, ip)$
18:    $smp = b_1/a_1$
19:    $\mathrm{image}(I_0)$
20:    $\mathrm{colormap}(cmap)$
21:    $divs \leftarrow \mathrm{size}(a_1)$
22:    $pp \leftarrow 0.01$
23:    **for** i=1:divs(1) **do**
24:        **for** j=1:divs(2) **do**
25:            **if** $S_{01}(i,j) > pp$ **then**
26:                **if** $smp(i,j) > pp$ and $hp_1(i,h) < 0$ **then**
27:                    ecolor $\leftarrow$ orange   ▷ Circular right
28:                **else if** $smp(i,j) > pp$ and $hp_1(i,h) > 0$ **then**
29:                    ecolor $\leftarrow$ green   ▷ Circular left
30:                **else if** $smp(i,j) \leq pp$ **then**
31:                    ecolor $\leftarrow$ white   ▷ Linear
32:                **end if**
33:                $\phi_2 \leftarrow \mathrm{mod}(\phi_1(i,j), 2\pi) \cdot 180°/\pi + 90°$
34:                drawellipse($'Center', [ip(j), ip(i)], 'SemiAxes', [b_1(i,j), a_1(i,j)],$
                                $'RotationAngle', \phi_2, 'color', \mathrm{ecolor})$
35:            **end if**
36:        **end for**
37:    **end for**
38: **end procedure**

---

beam intensity and draw it with the color assigned: orange to circular right, green to circular left and, white to linear polarization ellipse. To do this, in the **for** loop we have two conditions: the first one to determine if it is linear or circular and the second one to assign the handedness. Some note about the **Algorithm 4**

(a) Line 5: The total intensity, S_0 is given by the square root of sum of the square of the other Stokes parameters as we developed in equation 1.106.

(b) Line 7: The complex intensity of linear polarization had been described previously in equation 1.117.

(c) Line 8 to Line 11: The theory was presented in subsection 1.4.3 Stokes parameters and their relationship with polarization ellipse.

(d) Line 12: The command round round to the nearest integer all the entries in the vector of length samp.

(e) Line 13 and Line 14: Delimits the sampling area and resizes it by a scale factor, le.

(f) Line 15 to Line 17: Delimits the sampling area in a matrix of size $ip \times ip$

(g) Line 18: Divides the semi-minor axis by the semi-major axis to obtain information about the eccentricity of the ellipse.

(h) Line 21: Determine the number of divisions in the image once a_1 is given.

(i) Line 22: The value of pp is selected because it gives a suitable size and number of the drawn ellipses

(j) Line 33: Calculate the rotation angle of the ellipse

(k) Line 34: Draw a colored ellipse in each section analyzed where the center is given by the coordinates $O(ip_j, ip_i)$ with semi-axes $a_1(i, j)$ and $b_1(i, j)$ rotated by an angle ϕ_2

An example of what type of figure generates the **Algorithm 4** is shown in Figure A.3 where we can see the intensity profile, which is a vortex, with linear polarization distributed azimuthally. Here, the algorithm to generate the mosaic with the intensity for each Stokes parameter is the same

——— Some notes about **Algorithm 5** are

Algorithm 5 Partially Coherent Vector Beam Intensity

1: **procedure** PCVB-Part I($H, V, pxSize, \lambda, W_0, m, p, \alpha, \delta, RandomPositionCircle.$)
2:     H ▷ Horizontal image size in pixels
3:     V ▷ Vertical image size in pixels
4:     $x \leftarrow \text{linspace}(-(H/2), (H/2) - 1, H)$
5:     $y \leftarrow \text{linspace}(-(V/2), (V/2) - 1, V)$
6:     $pxSize$ ▷ Pixel size to scale the image
7:     $x \leftarrow x \cdot pxSize$
8:     $y \leftarrow y \cdot pxSize$
9:     $[X, Y] \leftarrow \text{meshgrid}(x, y)$
10:     λ ▷ Wavelength
11:     W_0 ▷ Waist radius
12:     z ▷ Direction of wave traveling
13:     m ▷ Indice
14:     p ▷ Indice
15:     α ▷ Weight factor (0 to $\pi/2$)
16:     δ ▷ Intermodal phase (0 to π)
17:     $R_0 \leftarrow \text{zeros}(H, V)$
18:     $L_0 \leftarrow \text{zeros}(H, V)$
19:     $H_0 \leftarrow \text{zeros}(H, V)$
20:     $D_0 \leftarrow \text{zeros}(H, V)$
21:     $\text{RandomPositionCircle}(N, c, h, k)$
22:     **for** i=1 $\rightarrow$ N **do**
23:         $X = X_0 - x_0(i);$
24:         $Y = Y_0 - y_0(i);$
25:         $u_1 \leftarrow \text{BeamFunction}(H, V, x, y, even, m, p, W_0, \lambda, z)$
26:         $u_2 \leftarrow \text{BeamFunction}(H, V, x, y, odd, m, p, W_0, \lambda, z)$
27:         $E_R = \cos\alpha \cdot u_1$
28:         $E_L = \exp(i\delta)\sin\alpha \cdot u_2$
29:         $E_H = (E_L + E_R)/\sqrt{2}$
30:         $E_D = (E_H + E_V)/2$
31:         $I_L = E_L \cdot E_L^*$
32:         $I_R = E_R \cdot E_R^*$
33:         $I_H = E_H \cdot E_H^*$
34:         $I_D = E_D \cdot E_D^*$
35:         $L_0 = L_0 + I_L$
36:         $R_0 = R_0 + I_R$
37:         $H_0 = H_0 + I_H$
38:         $D_0 = D_0 + I_D$
39:         $S_{00} = R_0 + L_0$ ▷ Total intensity
40:         $\text{StokesParameters}(S_{00}, R_0, L_0, H_0, D_0)$
41:     **end for**
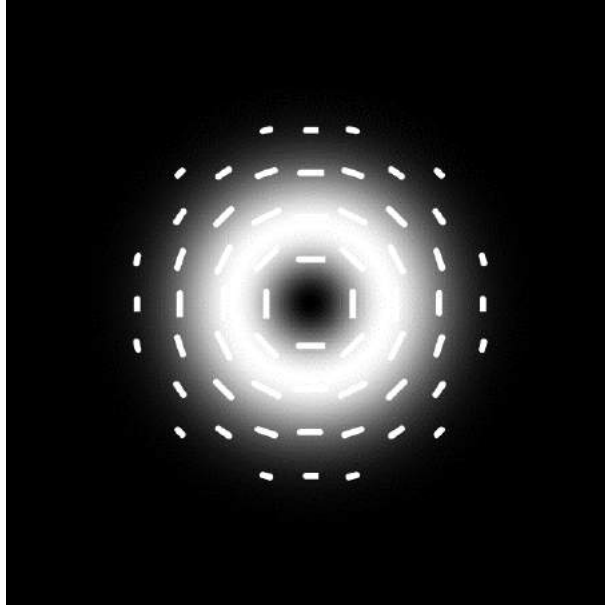42: **return** $L_0, R_0, H_0, D_0, S_{00}, S_1, S_2, S_3 S_0, S_1, S_2, S_3$

Figure A.3: Intensity profile with polarization distribution of a LG(1,0) vector beam with with $\alpha = \pi/4$ and $\theta = \pi/2$

Algorithm 6 PCVB-Part II

43:     le
44:     N
45:     StokesEllipses($S_0, S_1, S_2, S_3, n, le, cmap$)
46: **end procedure**

(a) Line 17 to Line 20: A $H \times V$ matrix full of zeros was create for each variable: R_0 is for right, L_0 for left, H_0 is for horizontal and D_0 is for diagonal.

(b) Line 21: RandomPositionCircle is used to generate the N random positions of the center of the beams.

(c) Line 22: The **for** loop is used to compute and do the superposition of the N beams

(d) Line 23 and Line 24: The new center of each beam X, Y is defined by the subtraction of the original position $(X_0, Y_0$ minus the coordinates generated by the function RandomPositionCircle, x_0, y_0.

(e) Line 35 to Line 38: The previous defined matrix full of zeros now is going to be filled with an accumulative sum of each component of the intensity in each one of the components.

(f) Line 40: The **Algorithm 3** is going to be used to calculate the Stokes parameters and generate a figure with four images, one for each parameter. Since it is inside the **for** loop, N-images will be generated that will allow us to see how the intensity of each Stokes parameter changes as the number of superposed beams increases.

(g) Line 45: The **Algorithm 4** is added to generate the intensity and polarization distribution image.

Bibliography

[1] Eugene Hecht. *Optics*. Pearson Education India, 2012.

[2] Dennis H. Goldstein. *Polarized Light*. CRC Press, 3 edition, 2011.

[3] Adad Yepiz, Benjamin Perez-Garcia, and Raul Hernandez-Aranda. Partially coherent ince-gauss beams. *Optics Letters*, 45(12):4 pp, 2020.

[4] et al Yangjian Cai. *Vectorial Optical Fields, Chapter 7: Partially coherent vector beams from theory to experiment*. University of Dayton USA. World Scientific, 2014.

[5] Benjamin Perez-García, Adad Yepiz, and Raul Hernandez. Structured light in the spatial coherence regime. *J. Opt.*, 24(044003):8pp, 2022.

[6] George Gabriel Stokes. On the composition and resolution of streams of polarized light from different sources. *Mathematical and Physical Papers*, page 233–258, 2009.

[7] Daniel F. James. Change of polarization of light beams on propagation in free space. *Journal of the Optical Society of America A*, 11(5):1641, 1994.

[8] Franco Gori. Matrix treatment for partially polarized, partially coherent beams. *Optics Letters*, 23(4):241, 1998.

[9] Emil Wolf. Unified theory of coherence and polarization of random electromagnetic beams. *Phys. Lett. A*, 312:263–267, 2003.

[10] Olga Korotkova. Scintillation index of a stochastic electromagnetic beam propagating in random media. *Optics Communications*, 281(9):2342–2348, Dec 2008.

[11] Fei Wang, Xianlong Liu, and Yangjian Cai. Propagation of partially coherent beam in turbulent atmosphere: A review (invited review). *Progress In Electromagnetics Research*, 150:123–143, Feb 2015.

[12] Tatiana Alieva, Alejandro Camara, and Jose A. Rodrigo. Synthesis and characterization of complex partially coherent beams. *Proc. of SPIE*, 9369(93690K):8pp, 2015.

[13] Xianlong Liu, Jun Zeng, and Yangjian Cai. Review on vortex beams with low spatial coherence. *Advances in Physics: X*, 4(1):1626766, 2019.

[14] Hao Zhang, Haiyun Wang, Xingyuan Lu, Xuechun Zhao, Bernhard J. Hoenders, Chengliang Zhao, and Yangjian Cai. Statistical properties of a partially coherent vector beam with controllable spatial coherence, vortex phase, and polarization. *Optics Express*, 30(17):29923, 2022.

[15] D. M. Palacios, I. D. Maleev, A. S. Marathay, and G. A. Swartzlander. Spatial correlation singularity of a vortex field. *Physical Review Letters*, 92(14), 2004.

[16] Yahong Chen, Fei Wang, Chengliang Zhao, and Yangjian Cai. Experimental demonstration of a laguerre-gaussian correlated schell-model statistical properties beam. *Optics Express*, 22(5):5826, 2014.

[17] Stuti Joshi, Saba N. Khan, P. Senthilkumaran, and Bhaskar Kanseri. Statistical properties of partially coherent polarization singular vector beams. *Physical Review A*, 103(5), 2021.

[18] Haidan Mao, Yahong Chen, Chunhao Liang, Linfei Chen, Yangjian Cai, and Sergey A. Ponomarenko. Self-steering partially coherent vector beams. *Optics Express*, 27(10):14353, 2019.

[19] José A. Rodrigo and Tatiana Alieva. Rapid quantitative phase imaging for partially coherent light microscopy. *Optics Express*, 22(11):13472, 2014.

[20] Malvin Teich Bahaa Saleh. *Fundamentals of photonics*. Wiley, 3 edition, 2019.

[21] Rüdiger Paschotta. Optical intensity, Apr 2023.

[22] Uri Levy, Stanislav Derevyanko, and Yaron Silberberg. Chapter four - light modes of free space. volume 61 of *Progress in Optics*, pages 237–281. Elsevier, 2016.

[23] Andreas Freise and Kenneth Strain. Interferometer techniques for gravitational-wave detection. *Living Reviews in Relativity*, 13 (1):5–48, 2010.

[24] Miguel A. Bandres and Julio C. Gutiérrez-Vega. Ince–gaussian beams. *Optics Letters*, 29(2):144–146, 2004.

[25] Joel B. Bentley, Jeffrey A. Davis, Miguel A. Bandres, and Julio C. Gutiérrez-Vega. Generation of helical ince-gaussian beams with a liquid-crystal display. *Optics Letters*, 31(5):649, 2006.

[26] Carlos López-Mariscal and Julio C. Gutiérrez-Vega. Propagation dynamics of helical hermite-gaussian beams. *SPIE Proceedings*, 2007.

[27] Carmelo Rosales-Guzmán, Xiao-Bo Hu, Valeria Rodríguez-Fajardo, Raul I Hernandez-Aranda, Andrew Forbes, and Benjamin Perez-Garcia. Experimental generation of helical mathieu–gauss vector modes. *Journal of Optics*, 23(3):034004, 2021.

[28] K. Sharma. *OPTICS. Principles and Applications*. Elsevier, 2006.

[29] Frank L Pedrotti, Leno M Pedrotti, and Leno S Pedrotti. *Introduction to optics*. Cambridge University Press, 2017.

[30] Richard Barakat. Analytic proofs of the arago–fresnel laws for the interference of polarized light. *Journal of the Optical Society of America A*, 10(1):180, 1993.

[31] Keshaan Singh, Najmeh Tabebordbar, Andrew Forbes, and Angela Dudley. Digital stokes polarimetry and its application to structured light: Tutorial. *Journal of the Optical Society of America A*, 37(11), 2020.

[32] Max Born and Emil Wolf. *Principles of optics*. Pergamon Press, 1980.

[33] Yu-Xuan Ren, Rong-De Lu, and Lei Gonf. Tailoring light with a digital micromirror device. *Annalen der physik*, 527, No 7-8(7-8):447–470, 2015.

[34] Mitchell A. Cox. Structuring light with digital micro-mirror devices. *Complex Light and Optical Forces XV*, 2021.

[35] N.A Correa-Rojas, R.D Gallego-Ruiz, and M.I Alvarez-Castaño. Generation of linearly polarized modes using a digital micromirror device and phase optimization. *Computer Optics*, 46 (1):30–38, 2022.

[36] Carmelo Rosales-Guzmán and Andrew Forbes. How to shape light with spatial light modulators. *SPIE Press*, 30, 2017.

[37] Carmelo Rosales-Guzman. *Photonic applications based on the use of structured light.* PhD thesis, The Institute of Photonic Sciences, 2015.

[38] Carmelo Rosales-Guzman. *Analysis of the Orbital Angular Momentum in Colliding Airy-Statistical properties beams.* PhD thesis, Instituto Nacional de Astrofísica, Optica y Electrónica, 2010.

[39] Giovanni Milione. *Vector beams for fundamental physics and applications.* PhD thesis, City University of New York, 2016.

[40] Yijie Shen, Shankar Pidishety, Isaac Nape, and Angela Dudley. Self-healing of structured light: A review. *Journal of Optics*, 24(10):103001, 2022.

[41] Edgar Medina-Segura, Leonardo Miranda-Culin, Valeria Rodríguez-Fajardo, Benjamin Perez-Garcia, and Carmelo Rosales-Guzmán. Helico-conical vector beams. *Optics Letters*, 48(18):4897, 2023.

[42] Carmelo Rosales-Guzmán, Bienvenu Ndagano, and Andrew Forbes. A review of complex vector light fields and their applications. *Journal of Optics*, 20(12):123001, 2018.

[43] Andrew Forbes, Andrea Aiello, and Bienvenu Ndagano. Classically entangled light. *Progress in Optics*, page 99–153, 2019.

[44] Keshaan Singh, Isaac Nape, Amogh Manthalkar, Najmeh Tabebordbar, Carmelo Rosales-Guzmán, Shanti Bhattacharya, Andrew Forbes, and Angela L. Dudley. Polarization reconstruction with a digital micro-mirror device. *Laser Beam Shaping XX*, 2020.

[45] Yuanjie Yang, Yu-Xuan Ren, Mingzhou Chen, Yoshihiko Arita, and Carmelo Rosales-Guzmán. Optical trapping with structured light: A review. *Advanced Photonics*, 3(03), 2021.

[46] Benjamin Perez-Garcia, Francisco I Mecillas-Hernández, and Carmelo Rosales-Guzmán. Highly-stable generation of vector beams through a common-path interferometer and a dmd. *Journal of Optics*, 24(7):074007, 2022.

[47] Carmelo Rosales-Guzmán, Xiao-Bo Hu, Adam Selyem, Pedro Moreno-Acosta, Sonja Franke-Arnold, Ruben Ramos-Garcia, and Andrew Forbes. Polarisation-insensitive generation of complex vector modes from a digital micromirror device. *Scientific Reports*, 10(1), 2020.

[48] Ahmed B. Ayoub and Demetri Psaltis. High speed, complex wavefront shaping using the digital micro-mirror device. *Scientific Reports*, 11(1), 2021.

[49] Edward Collett. *Field Guide to Polarization*, volume FG05. SPIE, 2005.